HERON is jointly edited by:
STEVIN-LABORATORY of the department of Civil Engineering, Delft University of Technology, Delft, The Netherlands
and
INSTITUTE TNO for Building Materials and Building Structures. Rijswijk (ZH), The Netherlands.
HERON contains contributions based mainly on research work performed in these laboratories on strength of materials, structures and materials science.

Secretary:
G. J. van Alphen
Stevinweg 1
P.O. Box 5048
2600 GA Delft, The Netherlands
Tel. 0031-15-785919
Telex 38070 BITHD

HERON vol. 28 1983 no. 3

Contents

THE BEARING CAPACITY OF PRESTRESSED HOLLOW CORE SLABS

J. C. Walraven
W. P. M. Mercx
Delft University of Technology
Stevinweg 1, P.O. Box 5048, 2600 GA Delft, The Netherlands

The bearing capacity of prestressed hollow core slabs

1 Introduction

Prestressed hollow core slabs are often used in prefabricated buildings. The units can quickly be assembled to form extensive floor slabs, by simply filling the joints between them and, eventually, laying a topping. The system of slabs with a topping has been common practice for a number of years, whereas the applicability of slab assemblies without topping is a recent subject of research, predominantly within the scope of the development of demountable structures [4, 15, 17, 18].

The slab units can be manufactured by various methods, but the technique of extrusion on a long casting line is coming more and more into widespread use. The units, sawcut to length from long continuous strips, usually consist of plain concrete with several pretensioned strands.

The special method of production (extrusion) of the slab makes the incorporation of anchorage reinforcement and shear reinforcement difficult, if not impossible. Furthermore the concrete is necessarily of high strength (generally above 60 N/mm^2).

Despite the widespread use of these products it was not clear to what extent existing code provisions, which of course give only general specifications for the design and analysis of structural components, apply to specific units such as prestressed hollow core slabs. Therefore it was decided to carry out an experimental program which would supply the necessary basis for design rules.

Two series of tests were carried out. In 1979 twelve tests were performed on single slabs subjected to line loads with variable load-span to depth ratios, and on double slabs, coupled by filling the longitudinal joint, subjected to eccentric line loads and concentrated loads.

All these slabs failed in bending. In order to observe the various shear failure modes that might occur, a second series of tests was carried out in 1981: thirty tests were performed on slabs with varying cross-section, depth and prestressing steel, which were subjected to line loads with varying load-span to depth ratios. These experiments yielded valuable information on the behaviour of prestressed hollow core slabs in various respects. In this report detailed data of all the tests are given, and the theoretical background necessary to understand the behaviour is also dealt with.

2 Failure modes

With regard to the way in which prestressed hollow core slabs fail when overloaded, four principal modes are distinguished.

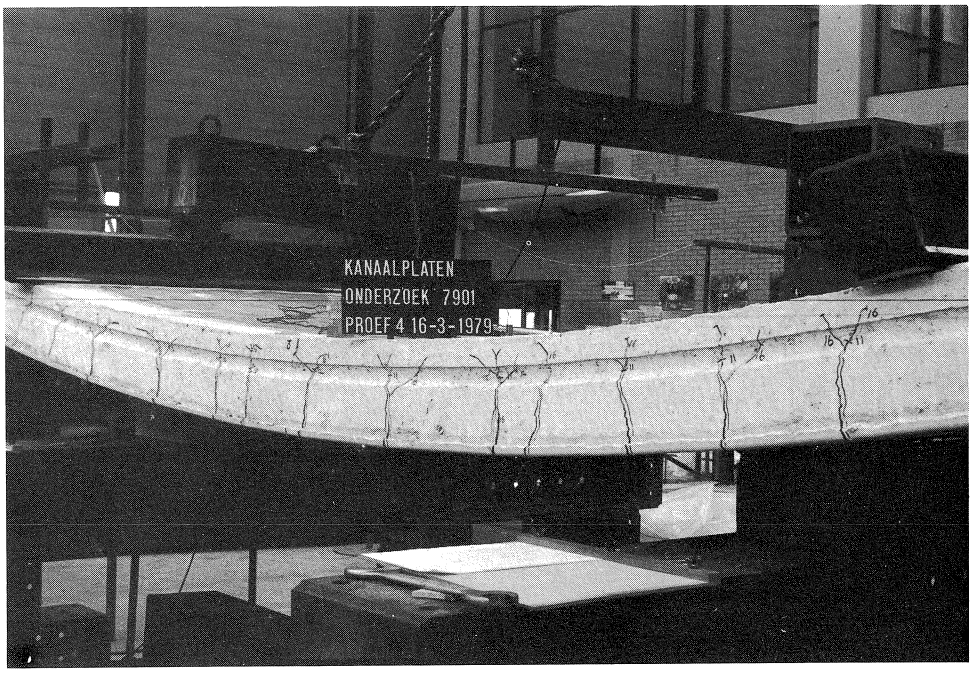

Fig. 2.1. Ductility after flexural cracking.

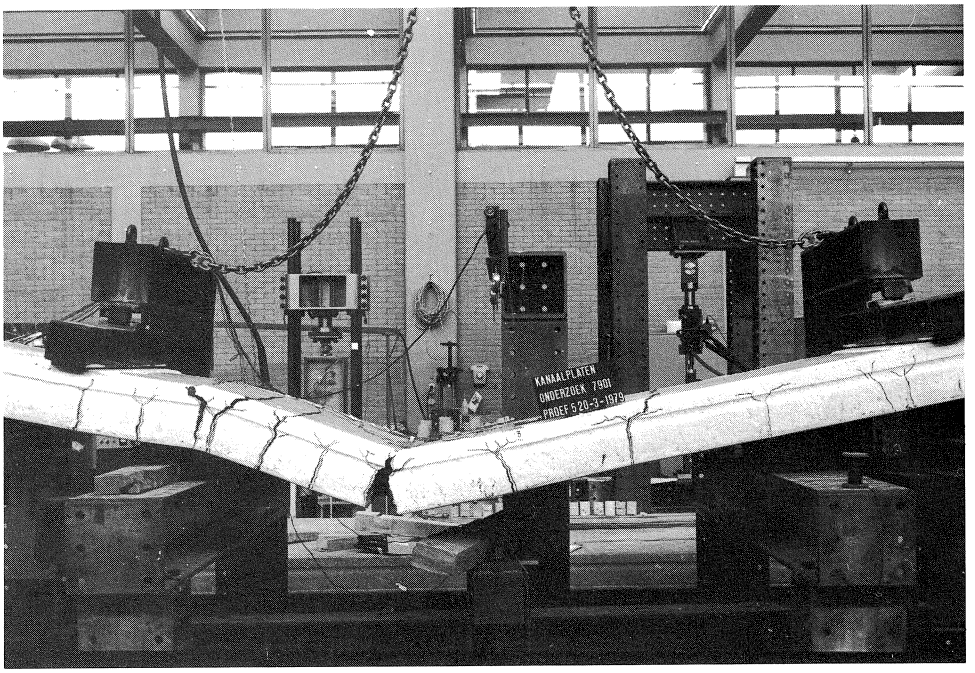

Fig. 2.2. Flexural failure.

2.1 *Behaviour in bending*

2.1.1 Pure flexural failure

Due to the relatively small cross-section of the steel the ductility of a slab after flexural cracking is considerable (Fig. 2.1).

Fork-shaped cracks develop, which reduce the compression area, but failure nevertheless generally occurs in consequence of rupture of the prestressing steel (Fig. 2.2).

2.1.2 Anchorage failure

If the cracking pattern extends too far towards the support a situation may occur in which the length of the anchored strand is too small to develop sufficient anchorage capacity; the strands slip through the concrete causing considerable widening of the cracks and large rotations (Fig. 2.3).

2.2 *Behaviour in shear*

2.2.1 Shear tension failure

If the tensile strength in the webs of the slab becomes too high in the region not cracked in bending, an inclined crack occurs, which propagates both in the upward and the downward direction, resulting in immediate failure. The crack is generally formed in

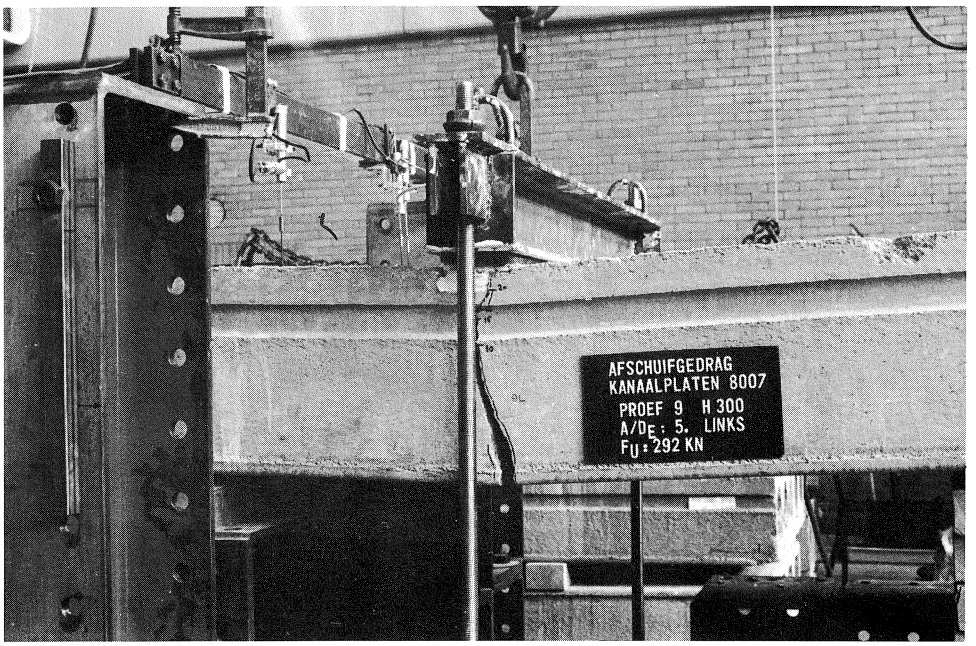

Fig. 2.3. Anchorage failure.

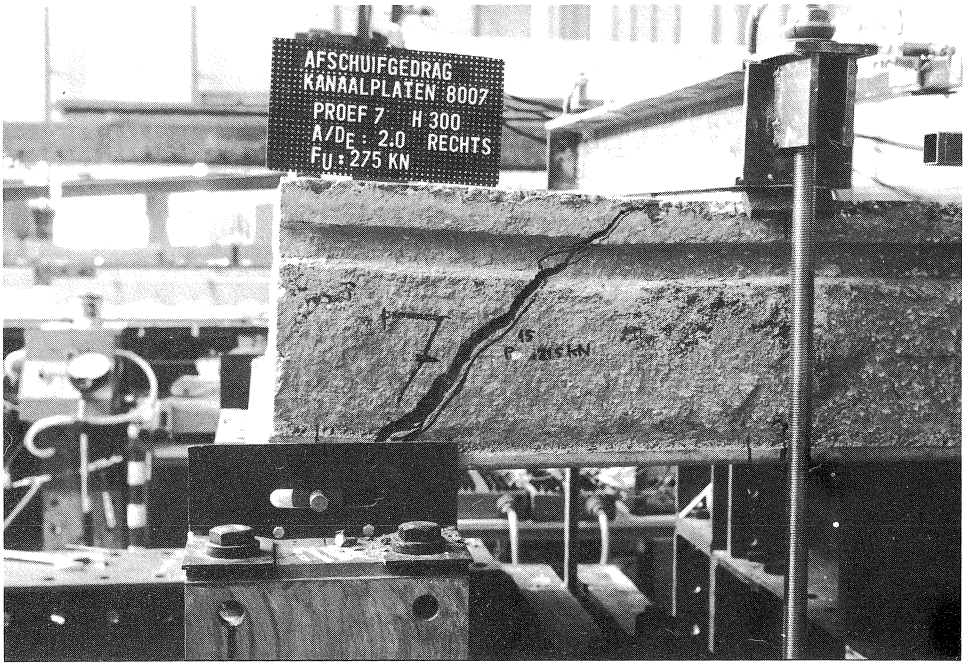

Fig. 2.4. Shear tension failure.

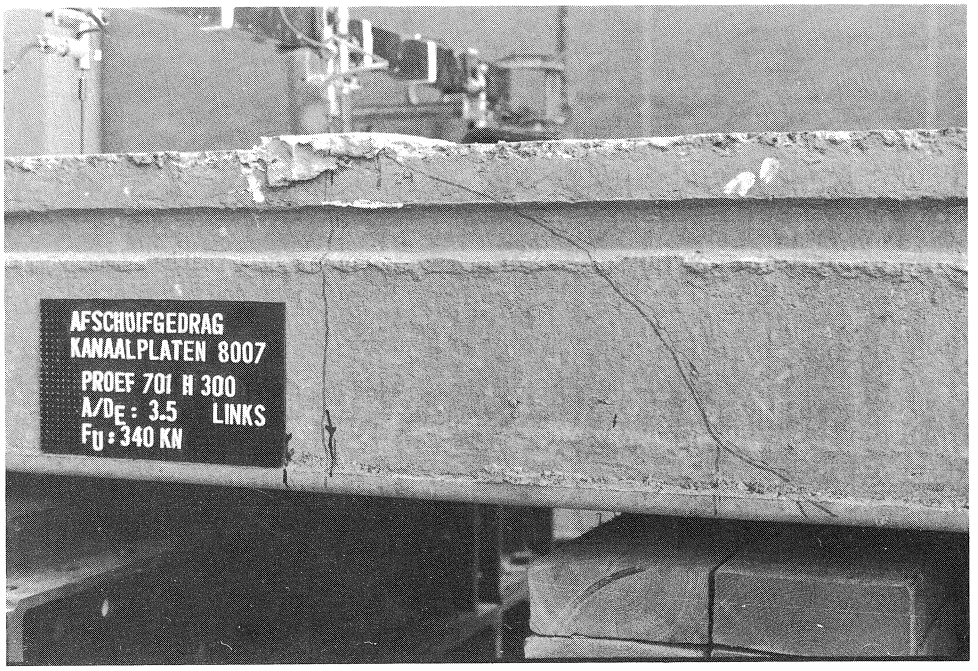

Fig. 2.5. Shear compression.

the region where the favourable influence of the vertical support stresses is exhausted and the prestressing force, which needs some length to develop, is not yet fully introduced (Fig. 2.4).

2.2.2 Shear compression failure

Flexural cracks can develop into shear cracks (Fig. 2.5). An increase of the load can subsequently result in failure of the compression zone, by crushing, or by splitting.

3 Theoretical background

3.1 *Pure flexural failure*

In the traditional approach to calculate the flexural moment capacity of a cross-section, it is assumed that in the compression zone the ultimate strain of the concrete is reached.

Using the σ-ε diagram for the concrete (Fig. 3.1) the ultimate moment can easily be calculated (Fig. 3.1b).

If it is assumed that the flexural crack reaches the upper flange of the slab, then the depth of the compression zone is calculated by:

$$A_p \cdot f_p = bx \cdot \lambda \cdot f_c \tag{3.1}$$

where λ is the shape factor of the stress-strain diagram of the concrete. The ultimate moment is then calculated from:

$$M_{fu} = (d - \beta x) \cdot A_p \cdot f_p \tag{3.2}$$

where d is the effective depth and βx is the distance from the centroid of the concrete compressive stresses to the top of the cross-section.

As mentioned in Section 2, prestressed hollow core slabs generally fail by rupture of the steel: this implies that actually the inner lever arm is somewhat smaller than found by the previous equations. For an accurate analysis the depth of the compression area x

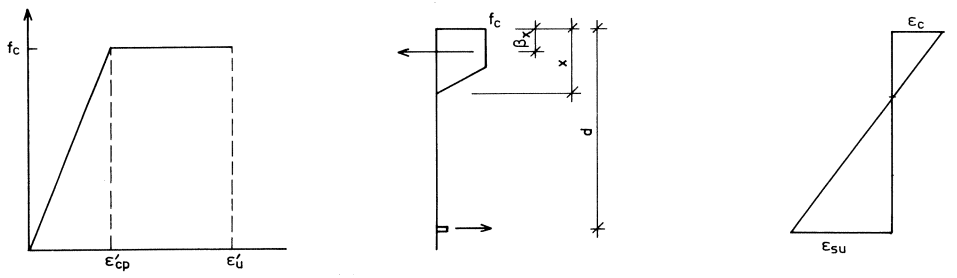

Fig. 3.1.

should be determined. This procedure is more complicated since the concrete in the compression zone may be in the non-linear state and the value of x may be large enough to reach the cavities of the cross-section. The differences between the accurate and the simple procedure for the hollow core cross-sections in practice are so small, however, (generally $< 2\%$) that the simple procedure can be used.

3.2 *Anchorage failure*

If a flexural crack is formed in the vicinity of a support, the force in the steel must be transmitted to the uncracked part of the member. If this part is too short the strands may start slipping and be pulled out under a nearly constant load.

To determine the anchorage capacity of strands it is useful to first consider how the prestressing force is introduced into the concrete at the end of the element. When a strand is released it will tend to shorten. As a result of the configuration of the wires, laid up around a central wire, the strand will develop frictional stresses while being drawn in. If these frictional stresses are sufficiently large, a limit state of equilibrium is reached and the strand stops slipping. The length necessary to develop the full prestressing force is called the transfer length l_t. Over this length the prestressing force builds up approximately according to a parabolic curve (Fig. 3.2).

If somewhere over the transfer length a flexural crack occurs it will hardly be possible to increase the stress in the steel, because of the limit state of equilibrium which exists in this area.

If a crack occurs just outside the transfer length an increase in the stress in the steel is possible. On both sides of the crack the stresses in the steel are raised over a certain length wich is sufficient to transmit the additional force in the strands, due to cracking, by bond stresses to the concrete. However, if the steel stress increase in the crack is so large that the flexural bond wave ((b), Fig. 3.2) invades the anchorage bond wave (a), the equilibrium over the transfer area is disturbed and the strands will start slipping. For any arbitrary cross-section a critical stress increment exists. If the distance to the end of the element is large enough the ultimate stress of the strands can be reached. This

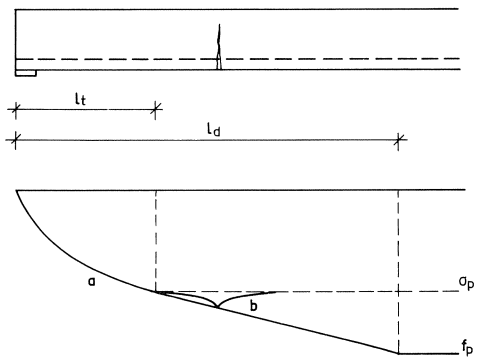

Fig. 3.2.

distance is denoted by the term "development length" (l_d). Experiments have shown that the curve representing the critical stress increase between the transfer length and the development length is approximately a straight line.

The length between the development length and the transfer length is called the flexural-bond length.

Limit curves for the stress in the strands are proposed by several authors.

The current ACI Code (318-71) [1], specifies that the transfer length be equal to:

$$l_t = \frac{(\sigma_{p\infty} \cdot \phi)}{21} \quad \text{(N, mm)} \tag{3.3}$$

and the development length:

$$l_d = \frac{\sigma_{p\infty} \cdot \phi}{21} + \frac{(f_p - \sigma_{p\infty}) \cdot \phi}{7} \quad \text{(N, mm)} \tag{3.4}$$

Zia and Mostafa [21] propose the values:

$$l_t = 1.5 \left(\frac{\sigma_{pi}}{f_{ci}} \right) \cdot \phi - 117 \quad \text{(N, mm)} \tag{3.5}$$

$$l_d = l_t + 0.179(f_p - \sigma_{p\infty}) \cdot \phi \quad \text{(N, mm)} \tag{3.6}$$

Martin and Scott [12] propose a transfer length of 80 diameters for strands of all sizes, and a flexural bond length of 160, 187 and 200 diameters for $\frac{1}{4}$, $\frac{3}{8}$ and $\frac{1}{2}$-inch diameter strands, respectively.

The critical stress envelope is defined as a bilinear curve. The stress at the break point (at l_t from the end of the element) is $\sigma_{p\infty}$ for [1, 21] and σ_{pi} for [12].

Fig. 3.3 shows a comparison of the envelopes for a specific case [21]. The bilinear envelope reflects the differences in bond properties between the subsequent areas. Over the transfer length the bond resistance is relatively large since the strands are in

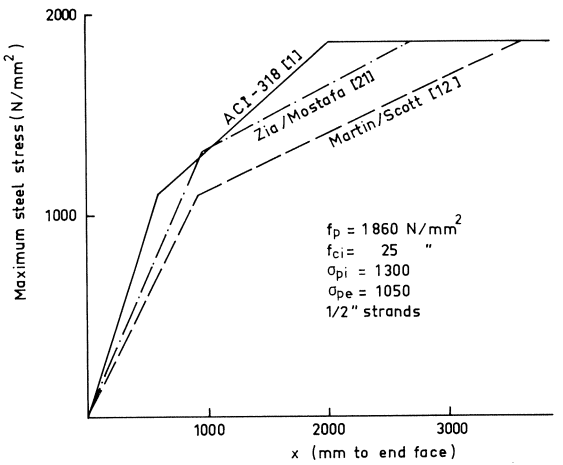

Fig. 3.3. Critical stress envelopes according to different proposals [21].

active frictional contact with the surrounding concrete. Over the flexural bond length the strands do not undergo a change in cross-section after release, so that only adhesion exists between the strands and the concrete; where the strands are stressed due to flexural cracking, the diameter diminishes, so that the adhesion is disrupted and the frictional forces which subsequently build up during sliding are relatively small. This explains the differences in slope of the lines defining the limit envelope.

In this report the formulae (3.3) and (3.4) will be used, in spite of the fact that these equations seem to be the least conservative (Fig. 3.3).

Anderson and Anderson [3] concluded on the basis of 36 tests on pretensioned hollow core units that these relations are adequate provided that the initial slip of the strands, upon the transfer of prestress, does not exceed an empirical value which is roughly 0.2 times the strand diameter.

The critical envelope being known, a lower bound value for the flexural, or pull-out, capacity of any cross-section can be calculated. In the following considerations two characteristic lengths will be used.

a. The development length l_d, beyond which the full flexural capacity can be reached: this length can directly be read in Fig. 3.4 or calculated from eq. (3.4).
b. The length l_{cr} between the end of the element and the cross-section where the increase of the stress in the steel upon cracking is just large enough to immediately reach the anchorage capacity. In order to simplify the calculation it will be assumed that the internal lever arm, when slip of the strands occurs, is equal to the distance from the strands to the mid-depth of the compression flange, at the lower side bounded by the top of the cavities.

With the values l_d and l_{cr} the general flexural behaviour can be represented quite simply.

For $x > l_d$ (Fig. 3.5) the full flexural capacity can be reached.

For $l_{cr} < x < l_d$ the capacity is larger than the flexural cracking moment but smaller than the full flexural capacity and is limited by slip of the strands.

For $x < l_{cr}$ the anchorage capacity is smaller than the flexural cracking moment, so that failure immediately occurs upon flexural cracking.

For $x < l_t$ it must be borne in mind that also the cracking moment is reduced due to the incomplete development of the prestressing force in that area.

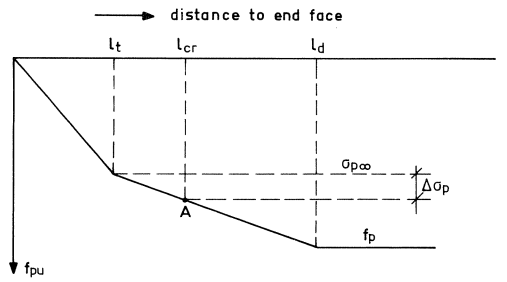

Fig. 3.4 Calculation of critical length l_{cr}.

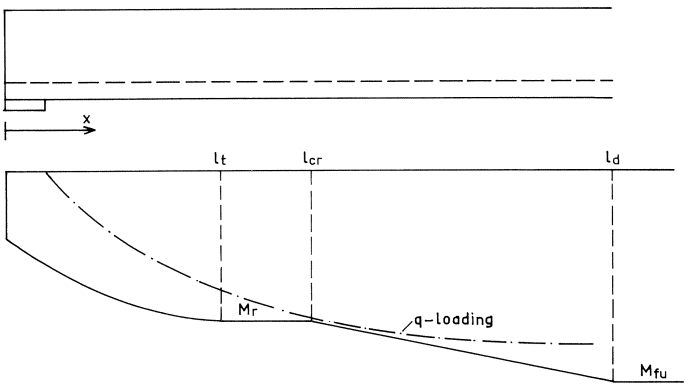

Fig. 3.5. Flexural and anchorage capacity along the length of an element.

If the load on an element is uniformly distributed the moment diagram is parabolic, so that the point l_{cr}, M_r may limit the bearing capacity (dotted line in Fig. 3.5). Whether this occurs or not depends upon the geometrical properties of the cross-section and the length of span between the supports.

If the element is subjected to a concentrated load, the bearing capacity depends always upon the ultimate moment which can be reached by the cross-section under the load.

3.3 *Shear tension failure*

3.3.1 General aspects of behaviour

Shear tension failure occurs if somewhere in the concrete the tensile stress reaches a critical value. This can be expected to occur outside the region where the vertical support pressure is active, but inside the region where the prestressing force is not yet fully developed.

Calculations of the stresses at the ends of beams with rectangular webs are found in the literature. In [7] the stress distribution is established by a FEM-calculation, in [16] using Airy's stress functions. However, in a hollow core slab the existence of circular cavities complicates the calculation. In order to obtain some insight into the behaviour at the end of the slab therefore a simplified approach has been choosen. A number of assumptions have been made.

a. *Stresses due to prestressing*

- The prestressing force in the transfer area is uniformly distributed over the width of the slab.
- The prestressing force is introduced into the concrete in increments $A_p \cdot \Delta\sigma_p$. Each increment of the force is transmitted by bond between steel and concrete over a length Δx, and spreads at 45 degrees.

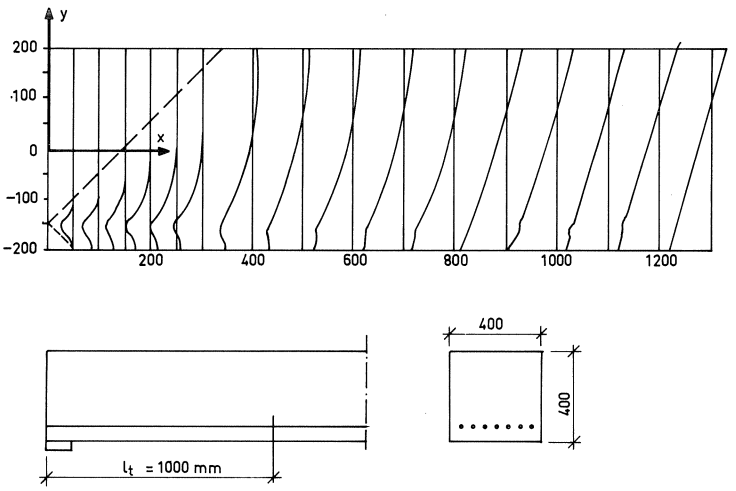

Fig. 3.6. Stresses in the concrete in the longitudinal direction for a rectangular cross-section.

- The prestressing force causes only stresses σ_{cxx} parallel to the longitudinal axis. The stresses σ_{cyy} and σ_{cxy} can be neglected.
- The stresses in the strands along the transfer length develop according to a parabolic curve.

Fig. 3.6 shows an example of the development of the stresses in the concrete, calculated in this way, for a rectangular cross-section.

b. *Stresses due to load*

The load on the member, including the dead weight, causes stresses σ_{xx} and σ_{xy}. The support pressure causes stresses σ_{yy}. Using the coordinate axes shown in Fig. 3.6, it is found that:

$$\sigma_{cxx} = -\frac{M_f}{I} \cdot y_1 \tag{3.7}$$

and

$$\sigma_{cxy} = \frac{V \cdot S(y)}{b(y) \cdot I} \tag{3.8}$$

A complication arises from the fact that the expression (3.8) comprises the shear stress acting perpendicularly to the plane of the slab. Along the edges of the holes this shear stress cannot act in that direction, because in that case a component perpendicular to the free edge would develop. In reality the direction of the shear stresses is approximately according to Fig. 3.7a. The value is such that the vertical component satisfies eq. (3.8). The maximum shear stresses occur along the edge; the direction of these stresses has been assumed to be as indicated in Fig. 3.7b. Only the maximum shear stresses, along the edge of the cavities, have been used in the analysis.

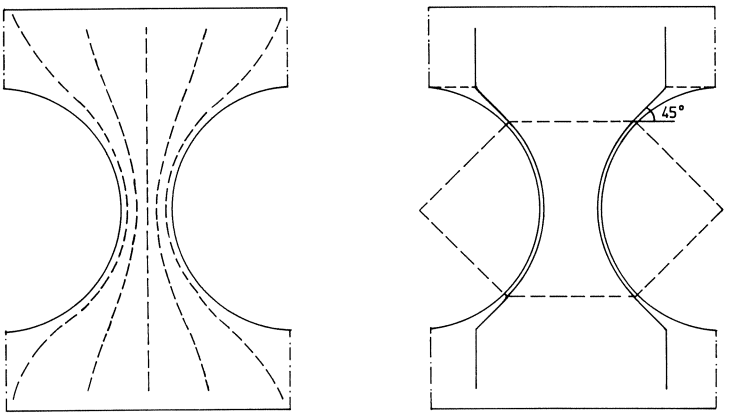

Fig. 3.7. Real and simplified shear stress distribution.

Further it is assumed that the support pressure spreads at an angle of 45 degrees. The vertical force to be transmitted by a horizontal section is assumed to be (Fig. 3.8):

$$F(y) = -\frac{V}{2} + \frac{V}{d_t} \cdot y \tag{3.9}$$

The section on which this force acts is then:

$$A(y) = b_w \left(s + \frac{d_t}{2} + y \right) \tag{3.10}$$

so that the vertical stress at the level y is:

$$\sigma_{cyy}(y) = \frac{F(y)}{A(y)} \tag{3.11}$$

The stresses as calculated at a number of points over the length of the element are superimposed, and the combined stresses are compared with the biaxial envelope according to [11] (Fig. 3.9).

In this way it is possible to determine the maximum capacity of any cross-section and the point where the critical combination of stresses is reached. Fig. 3.10 shows an exam-

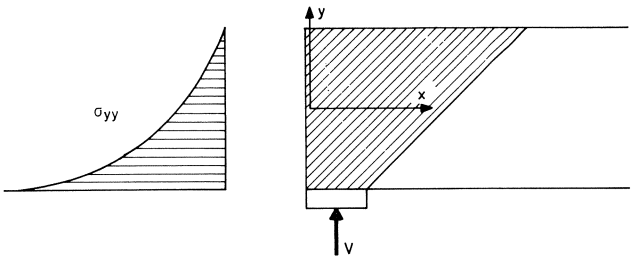

Fig. 3.8. Vertical stresses due to support reaction.

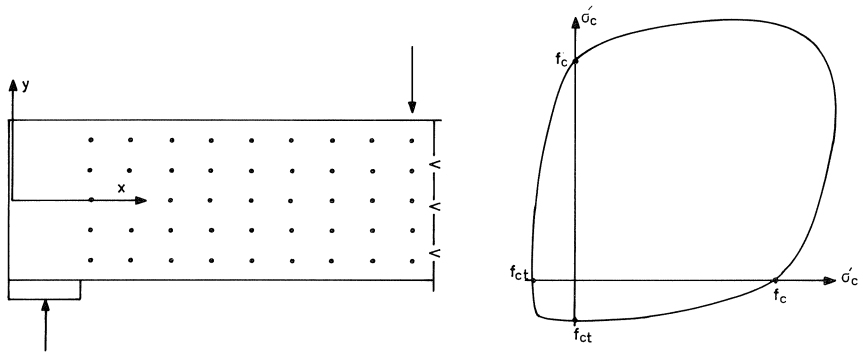

a. Reference points in member

b. Biaxial stress envelope, according to [11]

Fig. 3.9.

ple of such a calculation for a slab with a depth of 265 mm, and eight $\frac{3}{8}''$ strands with $l_t =$ 500 mm (for other cross-sectional properties see Fig. 4.6c). At a number of sections two critical points are found, which merely means that due to the size of the load increment the critical stress envelope is exceeded in two points at the same time. The minimum capacity of a section is nearly always reached at mid-depth, where the web width is a minimum.

The smallest capacity over the length of the member is reached where this plane is intersected by the plane inclined at 45 degrees from the inner edge of the support.

Since the critical stress combination in the centroidal plane does not depend upon the flexural moment, the capacity line between the support and the load is independent of the distance between them. So, theoretically, if the dead load is neglected so that the

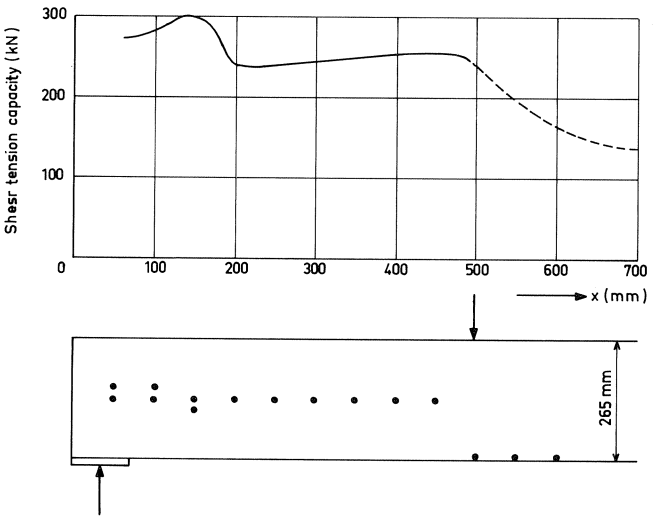

Fig. 3.10. Calculated shear tension capacity and critical point at a number of cross-sections.

shear force between support and load is constant, the shear tension capacity of the slab is independent of the shear span and is always reached at the section located at $d/2$ from the inner edge of the support.

In Fig. 3.10 it is shown that on the other side of the load the critical point is always reached at the bottom of the cross-section. This simply means that a flexural crack occurs, with no consequences to the failure capacity.

Fig. 3.10 shows that the shear tension capacity of the subsequent cross-sections does not differ very much. The differences may even be smaller if the transfer length is smaller and the support length is larger. Taking account of the scatter in concrete quality along the axis, it can be concluded that the shear tension crack will preferably occur at $d_t/2$ from the inner edge of the support, but may well occur elsewhere.

3.3.2 Simple formulation of shear tension capacity

It is assumed that the centroidal axis of the cross-section at $d_t/2$ from the inner edge of the support is the most probable location for a shear tension crack. It is further assumed that the prestressing force at the inner edge of the support determines the prestress in the concrete at the critical point (Fig. 3.11).

If the steel stress conforms to a parabolic curve, the stress at the inner edge of the support is:

$$\sigma_p(x=s) = \sigma_p \left\{1 - \left(\frac{l_t - s}{l_t}\right)^2\right\} = \alpha \cdot \sigma_p \tag{3.12}$$

and the compressive stress in the concrete at the critical point is:

$$\sigma_{cxx} = -\alpha \cdot \sigma_p \cdot \frac{A_p}{A_c} \tag{3.13}$$

The shear stress is:

$$\sigma_{cxy} = \frac{V \cdot S}{b_w \cdot I} \tag{3.14}$$

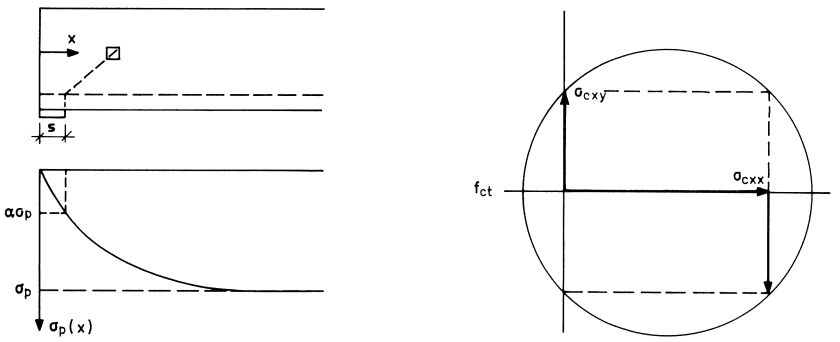

Fig. 3.11. Basis for simplified shear tension formulation.

If in the ultimate stress state the principal tensile stress is equal to the tensile strength of the concrete, then (Fig. 3.11b):

$$f_{ct} = \frac{\sigma_{cxx}}{2} + \sqrt{\left(\frac{\sigma_{cxx}}{2}\right)^2 + \sigma^2_{cxy}} \tag{3.15}$$

From eq. (3.13–3.15) it follows that:

$$V_u = \frac{b_w \cdot I}{S} \sqrt{f_{ct}^2 + \alpha \cdot \frac{A_p}{A_c} \cdot \sigma_p \cdot f_{ct}} \tag{3.16}$$

There are a number of reasons why eq. (3.16) can be expected slightly to overestimate the actual capacity:

- there is scatter in concrete quality along the axis of the member. Especially if the differences in shear tension capacity at the subsequent sections are small, the shear tension crack may search for the location with the smallest tensile strength; this would imply a dependence on the shear span a;
- the biaxial tension-compression stress combination may result in a reduced tensile strength;
- the value of σ_{cxx} (eq. (3.13)) may be slightly overestimated by using the prestressing force at the inner edge of the support;
- the period between the start of a test and failure is some hours. It is known that the tensile strength decreases under sustained load [2], which could even after a short time result in lower strength.

3.4 *Shear compression failure*

Shear compression failure occurs if a flexural crack develops into a shear crack which propagates through the member.

Factors affecting this mechanism are:

- the prestressing force, which delays the formation of a flexural crack;
- the reinforcement ratio, which influences the crack width and crack propagation;
- the concrete strength;
- the span-to-depth ratio (a/d): small span-to-depth ratios enable arch action to develop, provided that there is a well anchored reinforcing tie. In the case of pretensioned steel, however, the anchoring capacity of the strands will limit this influence, so that in this case arch action should not be taken into account;
- the depth of the section; from fracture mechanics it is known that unstable crack propagation occurs at a lower load if the crack is longer. Therefore the shear compression capacity is not proportional to the depth of the section but less.

On the basis of many experiments on reinforced and prestressed concrete Hedman and Losberg [8] derived a general empirical formula which takes account of these influences. They found that a 5% lower limit for the shear compression strength of members subjected to a concentrated load at a distance a from the support (Fig. 3.12) is

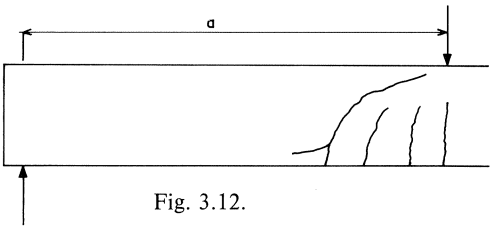

Fig. 3.12.

expressed by:

$$V_{uk} = 0.068 b_w \cdot d \cdot \xi (1 + 0.5 \varrho_0) \sqrt{f_c} + \frac{M_0}{a} \tag{3.17}$$

where:

$\xi = 1.6 - d \lessdot 1$, where d is expressed in meters

and

$$\varrho_0 = \frac{100 A_p}{b_w \cdot d}$$

It should be kept in mind that eq. (3.17) has been derived for beams with predominantly rectangular cross-sections.

In order to generalize eq. (3.17) so that it is applicable to any arbitrary loading configuration, the term M_0/a is replaced by $(M_x/V_x)M_0$, so that:

$$V_{uk} = 0.068 b_w \cdot d \cdot \xi (1 + 0.5 \varrho_0) \sqrt{f_c} + \frac{M_x}{V_x} \cdot M_0 \tag{3.18}$$

If the member is subjected to a concentrated load, shear compression failure will preferably occur in the vicinity of the load (Fig. 3.13a). If the load is uniformly distributed, failure occurs where the shear force at a section reaches the shear compression capacity (Fig. 3.13b). However, in the latter case there is a high probability that shear compression failure will not occur, because normally the shear tension capacity in the vicinity of the support is reached (Fig. 3.13c).

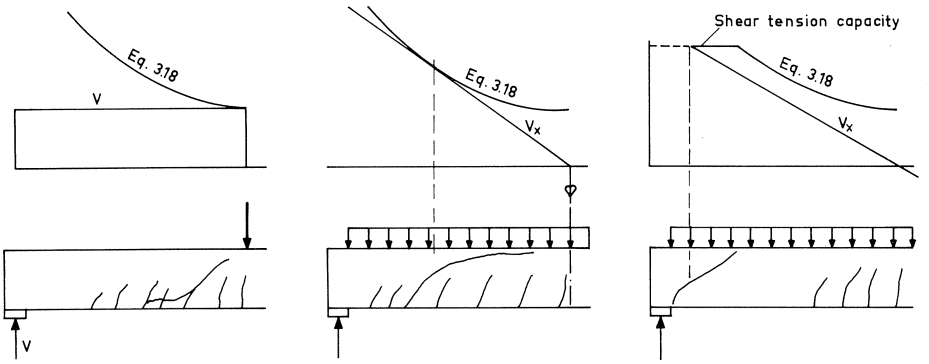

a, b. Shear compression failure in the case of concentrated (a) and distributed (b) loading

c. Shear tension capacity governing the behaviour

Fig. 3.13.

4 Experiments on prestressed hollow core slabs

4.1 *Series I* (1979)

4.1.1 Experimental set-up

Twelve tests were carried out on hollow core slabs with cross-sections as shown in Fig. 4.1. All slabs, except one, contained seven $\frac{3}{8}''$ strands (52 mm^2) according to Fig. 4.1a. The remaining one contained eleven $\frac{3}{8}''$ strands according tot Fig. 4.1b.

The slabs were of the Spiroll type and had been manufactured by Schokbeton at Alphen aan de Rijn.

Nine slabs were subjected to line loads over the full width of the unit, according to Fig. 4.2.

In all the tests the loading configuration was symmetrical with respect to the middle of the slab. The support length s was always 150 mm, the shear span a varied from 375 tot 3000 mm (Table 4.1).

Two slabs were subjected to a concentrated load applied over a circular area 200 mm in diameter (Fig. 4.3): in slab 10 this load was applied centrically (Fig. 4.3a), in slab 11 eccentrically (Fig. 4.3b).

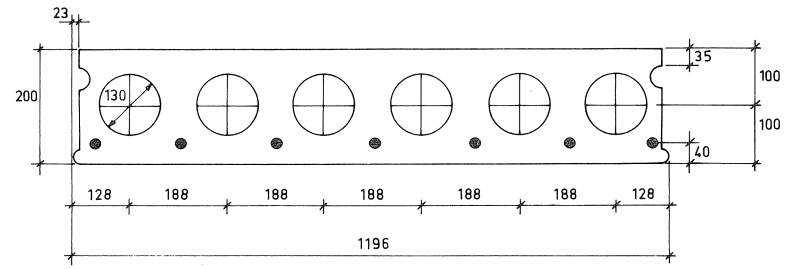

a SP 200 / 1200 – 7 strands

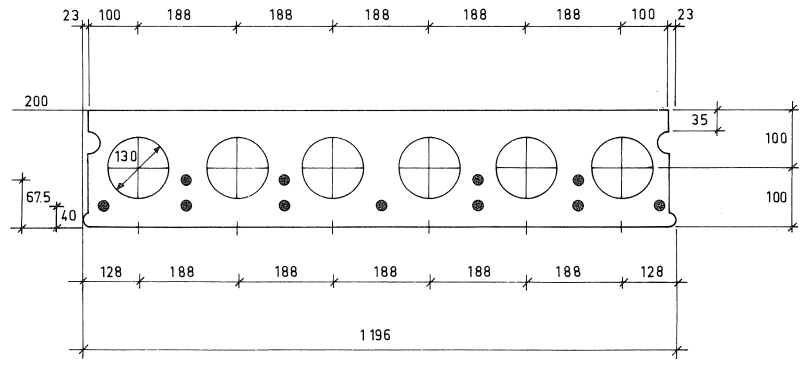

b SP 200 / 120– 11 strands

Fig. 4.1a, b. Cross-sections of extruded hollow core slabs loaded to failure.

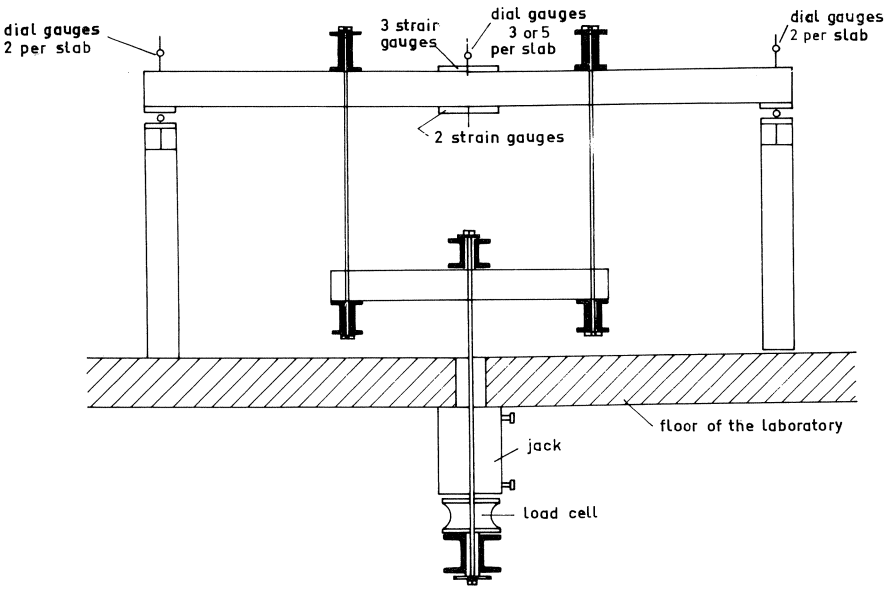

Fig. 4.2. Loading arrangement for series I.

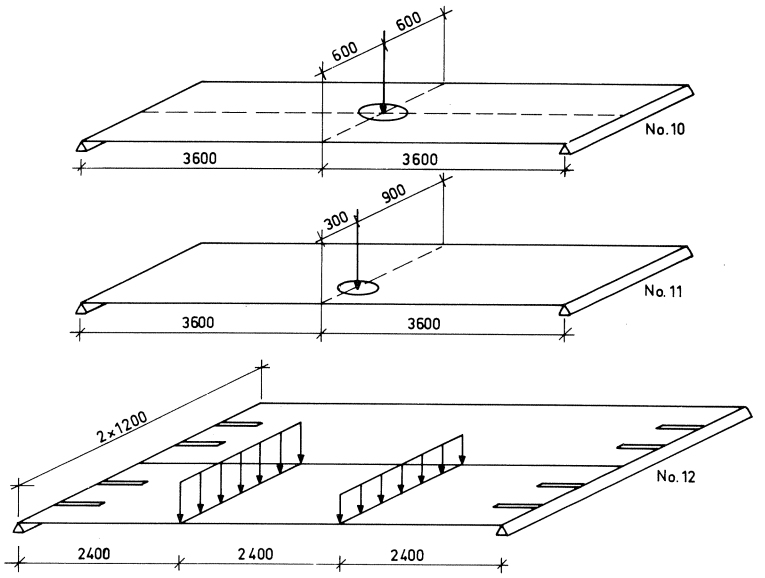

Fig. 4.3a-c. Tests on specimens 10, 11 and 12.

Table 4.1. Tests of series I.

test	span l (m)	shear span a (m)	a/d
1	5.40	1.80	11.2
2	7.20	2.50	15.6
3	9.00	3.00	18.7
4	6.00	1.50	9.4
5	5.00	1.00	6.2
6	4.50	0.75	4.7
7	4.00	0.50	3.1
8*	4.00	0.50	3.1
9	3.75	0.375	2.3

* 11 strands $\frac{3}{8}''$

One test was carried out on two coupled slabs: in this test the slab ends were provided with recesses. On assembly, reinforcement was installed, and the two slabs were interconnected by small end beams. The longitudinal joint was filled with mortar.

One of the beams was loaded according to Fig. 4.3c.

4.1.2 Properties of the specimens

Prestressing strands of steel grade FeP 1860 with a tensile strength of 1937–2010 N/mm^2 and a 0.02 per cent proof stress of 1810–1825 N/mm^2 were used.

The concrete compressive stress was measured on cubes made of the same mix as the slabs and treated in such a way that the same density was obtained. The average crushing strength of nine 150 mm cubes was 65.1 N/mm^2 with a standard deviation of $s = 0.38$ N/mm^2. The average splitting tensile strength was 5.1 N/mm^2 after 28 days, but decreased to 4.3 N/mm^2 after 56 and 90 days ($s = 0.15$), probably due to drying shrinkage. The flexural tensile strength of the concrete was measured on short slab sections ($l = 2200$ mm), without prestressing strands.

The flexural tensile strength was 5.75 N/mm^2, with a standard deviation of $s = 0.16$ N/mm^2. The average stress in the strands just before transfer, measured by a "Vogt Drahtspannungsmesser" (wire stress gauge), was 1240 N/mm^2 ($s = 24.5$ N/mm^2).

The maximum value of the draw-in of the strands at the end face of the unit, just before testing, had a maximum value of 0.5 mm for the inner strands and 1 mm for the strands at the edges of the cross-section.

The cross-sectional properties of the specimens are listed in Table 4.2.

Table 4.2. Cross-sectional properties, series I

I	710.5×10^6 mm^4
S	4.72×10^6 mm^3
W	7.23×10^6 mm^3
A_c	157×10^3 mm^2
d	200 mm
d_t	160 mm
b_w	370 mm

4.1.3 Results

All the specimens 1-9 failed in flexure.

The slabs 1-6 failed as a result of the maximum flexural resistance being exceeded. In all these cases there was fracture of all the prestressing strands. In slab 7 the five inner strands fractured at failure of the slab, while the two outer ones developed slip.

In the case of slab 8 (11 strands) slip of six strands was detected at one end of the slab (distance to nearest crack was 660 mm) when about 90 per cent of the ultimate failure load was reached, while two of the strands showed slip at the other end. Failure occurred as a result of nine of the strands fracturing at the first-mentioned end, while the two outer ones were pulled out of the concrete.

A tensile shear crack developed on the lateral face of slab 9. Closer inspection showed this crack to be present only in the outer wall of the cavity and to have been caused by incomplete filling between the slab and the load application beam, so that the load was transmitted mainly to the edge region of the slab. This defect was put right and the slab loaded again.

It finally failed in bending (flexural), with fracture of the five inner strands. The two outer strands had, as a result of the tensile cracking, ceased to be fully effective. The failure moment was about 10 per cent lower than the average moment of the comparable other slabs.

The tests 10 and 11 could be compared with 2, having the same span. The cracking moment was respectively 87 per cent and 84 per cent of the value obtained in test 2. The

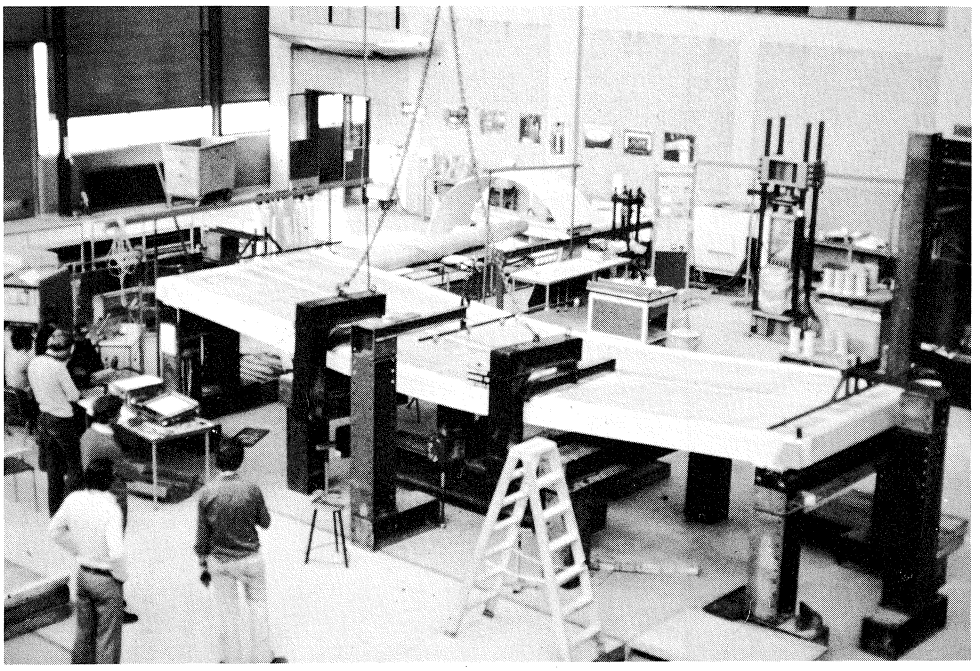

Fig. 4.4. Test on double slab.

respective values for the failure moment were 96 per cent and 101 per cent.

In the test on the double slab (12) it was found that initially the unloaded slab carried a 46–48 per cent share of the load, while the loaded slab carried 54–52 per cent. With the approach of failure the deflection of the two slabs at the joint was identical, and each slab was then carrying about 50 per cent of the load. Hence, in this case the failure load attained with the interconnected slab was about twice the failure load attained with one such slab with the same span. The joint remained undamaged. Fig. 4.4 shows the double slab during the test.

A survey of the flexural cracking and ultimate moments (including dead weight) is given in Table 4.3.

Table 4.3. Cracking and failure moments, observed in the tests

specimen	flexural cracking moment (kNm)	ultimate moment (kNm)
1	84.6	111.1
2	90.6	110.0
3	93.0	108.0
4	90.4	117.1
5	93.2	113.2
6	92.0	113.3
7	91.5	110.5
8	114.5	157.0
9	94.3	103.7
10	82.3	106.8
11	83.6	111.1
12	158.4	213.6

4.2 *Series II* (1982)

4.2.1 General

In series I only flexural failures had been observed, in spite of the large range of values for a/d (2.3–11.2).

In order to gather experimental evidence to verify the formulas for the other failure modes (shear tension, shear compression, anchorage failure) a fresh series of tests was scheduled, with not only the a/d value as a variable, but also the depth, the cross-sectional shape and the prestressing force. The slabs were of the types Dy-Core and Spiroll.

With a view to obtaining information with regard to anchorage failure the producer was requested to select a number of slabs with large initial drawn-in of the strands.

At a later stage similar slabs with regular, small, initial slip of the strands were subjected to similar loading conditions. The members with large initial slip are found in Table 4.8 under the numbers 1–3. The repeated series is found under the numbers 13–16.

4.2.2 Testing arrangement and instrumentation

The tests were carried out according to Fig. 4.5. The specimens were loaded by a single line load, which was asymmetrical with respect to midspan and was applied through a rigid transverse steel beam. In order to obtain a uniform distribution of the load over the width of the slab an intermediate layer of gypsum was applied between the loading beam and the element.

A layer of felt was interposed between the element and the supports. At the end where the roller bearing was situated the felt was applied over the full width of the slab; at the other end it was applied only over a short length in the middle of the slab. With the latter arrangement the element was able to rotate about the longitudinal axis, preventing unequal distribution of the support pressure at the loaded end.

The distance between the support and the load could be varied by shifting the support over the basis of the substructure.

The force applied by the jack was measured by a load cell. The deflection was measured at mid-span by three displacement gauges, distributed over the width of the element, so that any eccentricity could be registrated. Further on, the sagging at the supports due to compression of the supporting strips was measured in order to find the actual load-deflection relation. Before each test the draw-in of the middle wire of all the strands was measured. During testing, further slip was recorded by means of displacement gauges.

In order to detect the stress in the strands and the flexural tensile strength of the con-

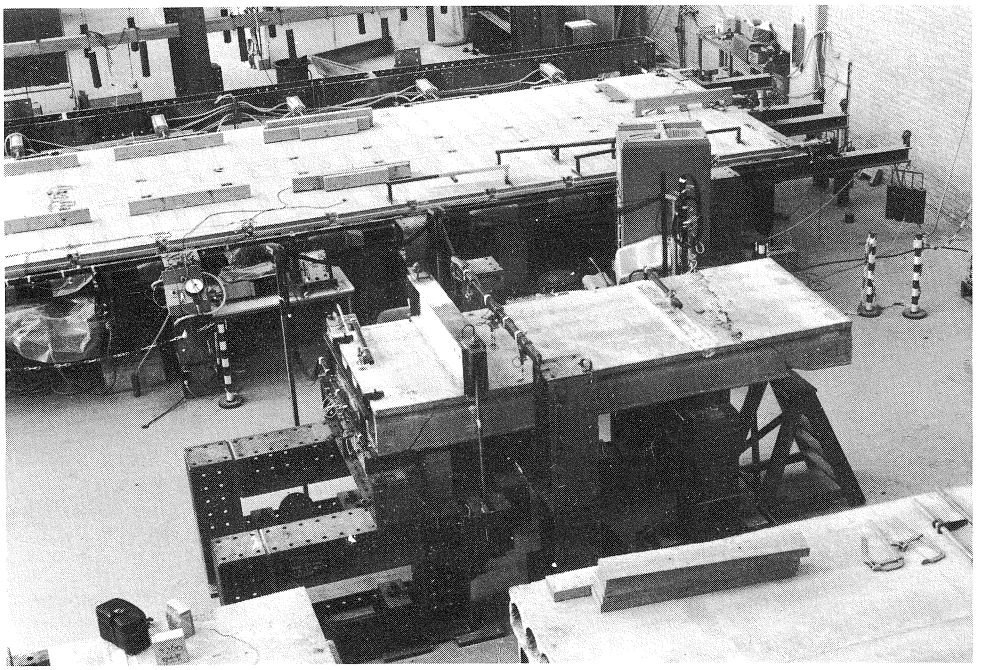

Fig. 4.5. Testing arrangement.

crete the decompression moment was measured. This was done by unloading after the first flexural crack had appeared and reloading: the value of the decompression moment was then read from the load-deflection curve. The flexural tensile strength and the prestressing force can be calculated from the flexural cracking moment and the decompression moment.

4.2.3 Variables

The tests comprised 20 specimens, 16 of which were Dy-Core slabs and four were of the Spiroll type. In the case of 10 of these slabs both ends were used, so that altogether 30 tests were carried out.

Slabs with three different cross-sections were tested; two of these contained two different numbers of strands. The cross-sections are shown in Fig. 4.6.

The geometrical properties are summarized in Table 4.4.

Table 4.4. Cross-sectional properties of specimens tested, series II

	T260		H 300		SP 270
strands	$6-\frac{1}{2}''$	$10-\frac{1}{2}''$	$5-\frac{1}{2}''$	$10-\frac{1}{2}''$	$13-\frac{3}{8}''$
A_c (mm^2)	1.71×10^5	1.71×10^5	1.99×10^5	1.99×10^5	1.78×10^5
b_w (mm)	294	294	250	250	260
S (mm^3)	6.61×10^6	6.61×10^6	9.72×10^6	9.27×10^6	7.66×10^6
I (mm^4)	1.34×10^9	1.36×10^9	2.18×10^9	2.23×10^9	1.55×10^9
A_p (mm^2)	564	940	470	940	676
d (mm)	225	225	265	260	230

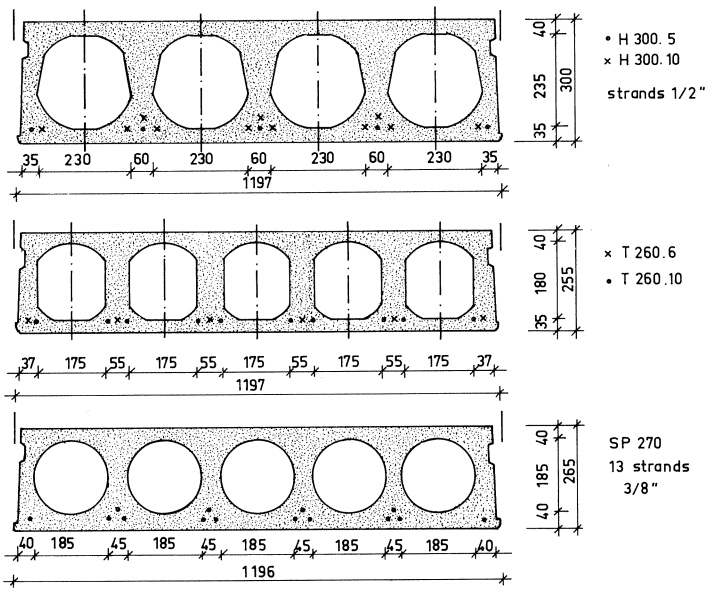

Fig. 4.6. Cross-sectional dimensions of the slabs tested.

A survey of all the tests, showing all combinations of parameters, is given in Table 4.8.

The slabs 1–3 displayed outward features, on the basis of which they should be withdrawn from sale: the mix was too dry, which was confirmed by the large initial slip of the strands in the slabs 2 and 3 ($\delta = 2.9$ and 3.8 mm, see Table 4.8). Nevertheless the quality of concrete, on visual inspection, was constant along the length of the specimens and the initial slip values of the strands in the saw cut were approximately equal. As a result of these properties the slabs were considered suitable for studying the relation between the initial slip of the strands upon sawing and the anchorage capacity of the strands. Slabs 13–16 had the same cross-sectional properties, but their quality was satisfactory. Slab 10 exhibited tensile splitting cracks around the outer strand in the rib and bottom and must also be rated as deficient in quality.

4.2.4 Material qualities

Concrete

It is normal practice that the producer of the slabs supplies cubes for quality control. However, with regard to the manner of casting, vibrating and curing a number of differences exist between the slabs and the cubes, which makes the quality control values disputable. Therefore, additionally, a large number of tests with a rebound hammer were performed.

The cube compression values for a number of slabs are represented in Table 4.5.

Table 4.5. Values of concrete crushing strength, measured on cubes, separately cast with concrete of the same batch

specimen	f_{cc} (N/mm^2)			$\bar{f}_{cc}$
1, 2, 3	64.2	62.2		63.2
7, 8, 9	66.1	67.9	69.2	67.7
10, 11, 12	54.5	54.6	46.1	51.7

The rebound values determined with a Schmidt Hammer were obtained at ten different locations both on the sides and on the end faces of the elements. The values converted to cube strength, for a number of specimens, including those from Table 4.5, are given in Table 4.6.

Table 4.6. Rebound values by Schmidt Hammer, converted to cube crushing values

specimen	f_{cc} (N/mm^2) side			$\bar{f}_{cc}$, side average	f_{cc} (N/mm^2) face			$\bar{f}_{cc}$, face average
1, 2, 3	60.7	58.7	48.6	56.0	62.1	62.2	63.0	62.6
7, 8, 9	57.1	65.5	59.2	60.6	61.8	66.1	62.5	63.5
10, 11, 12	53.2	58.9	55.4	55.8	63.1	66.7	66.7	65.5
14, 17	49.4	59.0		54.2	61.8	62.6		62.2

It appears that the values obtained on the sides are slightly lower than those obtained on the sawn end faces, which is explained by the larger area of particles encountered by the

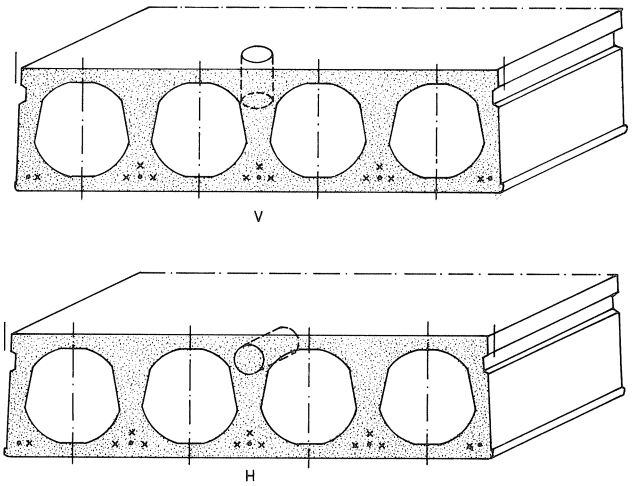

Fig. 4.7. Cylindrical cores were obtained for determining the splitting tensile strength of the concrete.

hammer. Except for the specimens 10–12, the values are in good agreement with those obtained in the direct cube tests.

From a number of specimens cylindrical cores 75 mm in diameter were taken in order to determine the tensile splitting strength. Vertical and horizontal cylinders were sawn, as indicated in Fig. 4.7.

According to [14] the cylinder diameter has no significant effect on the splitting tensile strength. The cylinder splitting tensile strength was calculated from the well known relation

$$f_{cts} = \frac{2P}{\pi \, \mathrm{d}l}$$

Table 4.7. Splitting tensile strength, determined on cylindrical cores

specimen	cylinder	f_{ct} (N/mm^2)
1b	vertical	2.8
	horizontal	1.9
3	vertical	4.3
	horizontal	3.3
7b	vertical	4.8
	horizontal	3.6
8	vertical	4.2
	horizontal	4.3
9	vertical	3.9
	horizontal	4.3

The values for the specimens 1 and 3, from the casting bed on which occasionally large initial slip of the strands was observed (Table 4.8), are considerably lower than those for the other, regular specimens. The average splitting tensile strength of the cores taken

from the specimens 7, 8 and 9 was 4.2 N/mm^2 with a standard deviation of $s = 0.4$ N/mm^2.

A direct relation between the tensile splitting strength and the cube crushing strength is [5]:

$$f_{ct} = 1 + 0.5 f_{cc} \tag{4.1}$$

A splitting tensile strength of 4.2 N/mm^2 corresponds to a cube crushing strength of 64 N/mm^2. Apparently there is good agreement between the splitting tensile strengh determined on cores and the crushing strength determined in cube tests and rebound tests.

Steel

In the specimens $\frac{1}{2}''$ strands with $A_p = 94$ mm^2 and a diameter of 12.5 mm as well as $\frac{3}{8}''$ strands with $A_p = 52$ mm^2 and a diameter of 9.5 mm were used. The steel grade was FeP 1860: the 0.02% proof stress was 1800 N/mm^2, the characteristic (5% lower bound) tensile strength 1860 N/mm^2, and the average tensile strength 2000 N/mm^2. The modulus of elasticity was between 200000 and 206000 N/mm^2.

4.2.5 Experimental results

Prestress in the strands and flexural tensile strength of the concrete

After the first flexural crack had occurred the specimen was unloaded and reloaded, so that the decompression moment could be measured. From the flexural cracking moment M_r and the decompression moment M_0 the flexural tensile strength of the concrete can be calculated from the relation:

$$f_{ctf} = \frac{(M_r - M_0)}{W} \tag{4.2}$$

The prestress in the steel σ_p is obtained from:

$$\sigma_p = \frac{M_0}{A_p \left(\frac{W}{A_c} + e \right)} \tag{4.3}$$

Considering the load deflection diagrams (Fig. 4.8) it was not always possible to find an exact value of the decompression load. Therefore for each case a lower and an upper value was estimated: the lower value of P_0 gives an upper limit value for f_{ctf} and a lower limit value for σ_p. In the same way the upper value of P_0 gives a lower limit value for f_{ctf} and an upper limit value for σ_p. These limit values are represented in Fig. 4.9 where the f_{ctf}-σ_p relations have been plotted.

The slabs 1b and 2, coming from the low-quality casting bed, show f_{ctf}-σ_p relations which significantly deviate from the regular ones. Indeed specimen 2 had an average initial slip of the strands equal to $\delta = 2.9$ mm. However, specimen 1b had the smallest initial slip of all specimens of the whole series II ($\delta = 0.0$ mm). The small value of σ_p

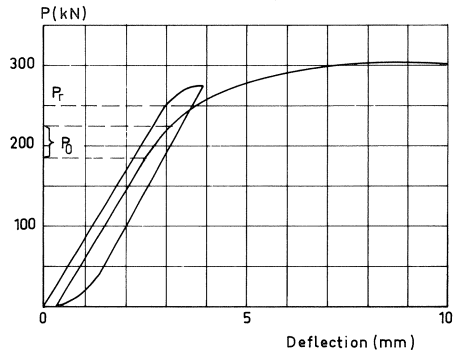

Fig. 4.8. Load-deflection diagram for specimen 14.

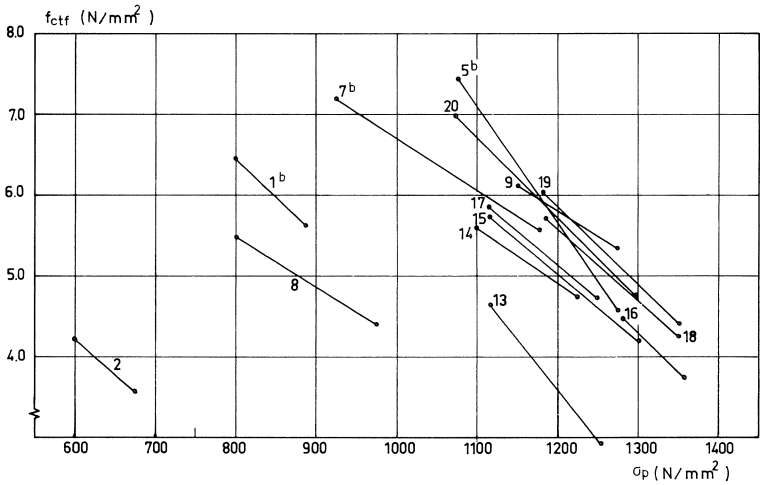

Fig. 4.9. f_{ctf}-σ_p relation as measured in the tests.

could be explained by the fact that slip over a large length had occurred due to bad compaction of the concrete in the adjacent slab already before the slab itself was sawn.

No explanation for the deviating behaviour of the specimens 8 and 13 was found: in both cases the slabs came from a regular casting bed and were apparently good.

Transmission of forces in the anchorage zone

In two slabs the transmission length was established by measuring the strain in the concrete. This was done in a special test. A 6 m long slab (T 260-6 strands $\frac{1}{2}''$) was turned upside down: on the surface six lines of reference points for strain measurement were stuck on the surface, covering a range of 1 m on both sides of the sawing cut. Subsequently the slab was sawn into two pieces (Fig. 4.10).

For this procedure the steel must be anchored, so that the concrete is partially destressed and elongates. The strain increments are represented in Fig. 4.11.

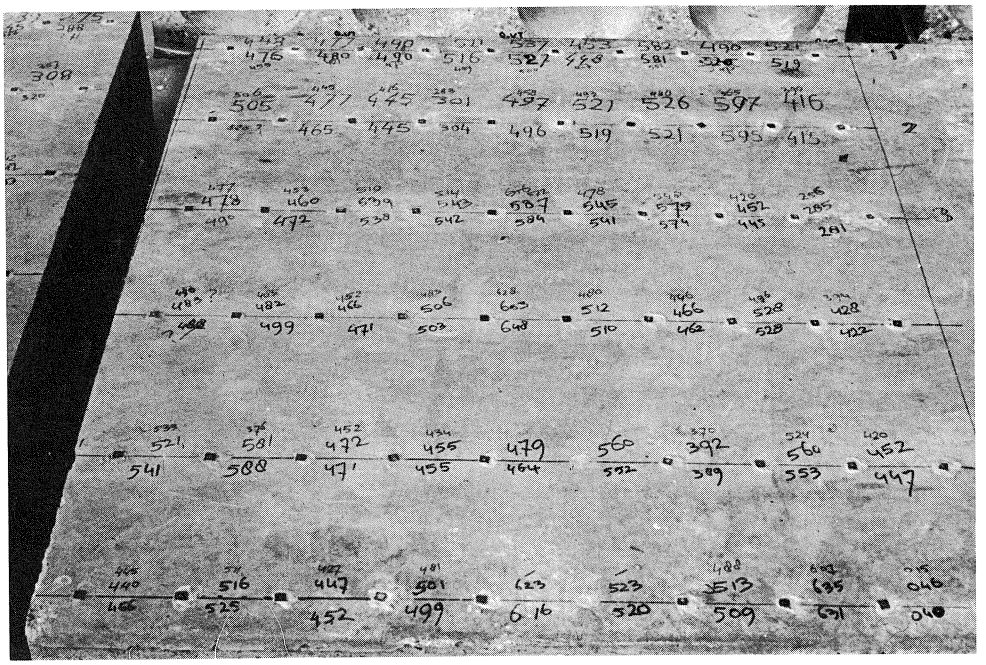

Fig. 4.10. Reference points on slabs 15 and 16, used to measure the transmission length of the strands.

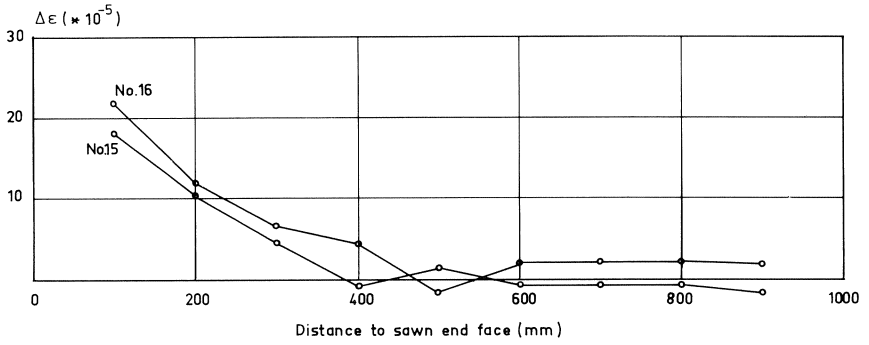

Fig. 4.11.

It is shown that a distance of 450–550 mm from the saw cut the influence of the sawing has vanished. The slip of the strands at both sides of the cut was found to be different. In slab 15 the average slip was 0.79 mm, whereas in slab 16 it was only 0.18 mm.

Ultimate resistance and failure modes

All data regarding the failure of the slabs have been collected in Table 4.8. If both ends of an element have been tested, this is indicated by an added letter e.g., the tests 1a and 1b were carried out at different ends of the same specimen. If the undamaged part of the

Table 4.8. Experimental results

test	type	strands	a (mm)	a/d	P_u (kN)	V_u (kN)	M_u (kNm)	M_r	δ_{av} (mm)	P_{slip}	failure mode
1a	T 260	6-$\frac{1}{2}''$	460	2.04	178.0	139.3	63.5	63.5	0.1	178.5	A*
1b	T 260	6-$\frac{1}{2}''$	805	3.58	306.5	204.0	162.7	138.0	0.0	259.4	A*
2	T 260	6-$\frac{1}{2}''$	1475	6.56	123.0	66.3	97.8	97.8	2.9/0.1	123.0	A*
3	T 260	6-$\frac{1}{2}''$	1150	5.11	123.2	75.3	83.7	83.7	3.8/0.5	123.2	A*
13	T 260	6-$\frac{1}{2}''$	1500	6.67	300.9	161.0	236.5	149.0	0.62/0.48		F
14	T 260	6-$\frac{1}{2}''$	1150	5.11	318.7	168.0	211.0	160.0	0.25	316.5	A/F
15a	T 260	6-$\frac{1}{2}''$	805	3.58	353.0	234.2	187.0	160.6	0.79		St
15b	T 260	6-$\frac{1}{2}''$	460	2.04	333.3	258.3	118.2		0.43		St
16a	T 260	6-$\frac{1}{2}''$	805	3.58	370.9	245.9	196.4	162.5	0.18	352.5	St
16b	T 260	6-$\frac{1}{2}''$	460	2.04	364.4	282.0	129.1		0.23		St
4a	T 260	10-$\frac{1}{2}''$	460	2.04	367.4	284.3	130.2		0.32		St
4b	T 260	10-$\frac{1}{2}''$	805	3.58	405.4	268.3	214.5		0.22		St
5a	T 260	10-$\frac{1}{2}''$	460	2.04	370.4	286.3	131.2		0.26		St
5b	T 260	10-$\frac{1}{2}''$	1150	5.11	435.5	252.1	287.0	240.4	0.12		St
6	T 260	10-$\frac{1}{2}''$	1500	6.67	413.5	213.3	314.9	249.7	0.43/0.58	252	St/L
7a	H 300	5-$\frac{1}{2}''$	540	2.04	277.5	216.0	115.9		0.36		St
7b	H 300	5-$\frac{1}{2}''$	945	3.57	368.7	231.5	216.0	186.9	0.40	317.5	St
8a	H 300	5-$\frac{1}{2}''$	945	3.57	271.0	171.5	160.0	151.3	0.50	256.0	A
8b	H 300	5-$\frac{1}{2}''$	440	1.66	230.7	181.6	79.3		0.9		St
9	H 300	5-$\frac{1}{2}''$	1500	5.66	299.3	156.6	229.6	190.7	0.9/0.9	247.5	F/A
10a	H 300	10-$\frac{1}{2}''$	540	2.08	278.8	208.5	111.8		0.31		St
10b	H 300	10-$\frac{1}{2}''$	945	3.63	237.7	151.1	140.6	140.6	0.26	237.7	A**
11a	H 300	10-$\frac{1}{2}''$	945	3.03	357.5	224.6	210.0		0.39		St
11b	H 300	10-$\frac{1}{2}''$	540	2.08	320.5	239.3	128.5		0.42		St
12	H 300	10-$\frac{1}{2}''$	1495	5.75	438.5	226.2	332.9	264.8	0.36/0.36	381.5	St
17	SP 270	13-$\frac{3}{8}''$	1500	6.52	368.0	190.9	281.0	192.8	0.30/0.31		F
18	SP 270	13-$\frac{3}{8}''$	1150	5.00	414.4	240.6	273.6	198.5	0.33/0.46	402.5	St
19a	SP 270	13-$\frac{3}{8}''$	805	3.50	417.2	276.3	220.8	200.6	0.5		St
19b	SP 270	13-$\frac{3}{8}''$	460	2.00	340.5	263.9	120.8		0.34		St
20	SP 270	13-$\frac{3}{8}''$	1150	5.00	414.9	240.8	270.3	200.6	0.71/0.4		A/F

* dowgraded elements
** splitting crack in outer rib

specimen was too short for another test, the values of the initial slip of the strands are given for both ends of the specimen. The first value applies to the loaded end. The failure mode is indicated by an identifying letter:

A = Anchorage failure
St = Shear-tension failure
F = Flexural failure

In specimen 6 a longitudinal crack occurred first. Then eccentric shear tension failure occurred, denoted by *St/L*. No shear compression failure was observed. In two specimens (13 and 17) a shear compression crack developed but did not cause failure.

P_u is the load at which failure occurred. V_u is the ultimate support reaction (including the dead weight of the specimen). P_{slip} is the load at which at first slipping of one or more strands was observed.

Nine failures were observed which displayed slip of one or more strands. In four cases (1a, 1b, 2 and 3) the load at which the first flexural crack occurred was also the maximum capacity: in the specimens 1b and 3 the strands kept on slipping at a load which was approximately equal to the cracking load; in specimen 1a and 2 the slipping load was respectively 15% and 6% smaller than the flexural cracking load. In specimen 10b there was a shrinkage crack in the outer rib before testing. Therefore the outer strand should not be taken into account in the analysis of the results. All the strands slipped.

In four cases the ultimate load was higher than the flexural cracking load (8a, 9, 14

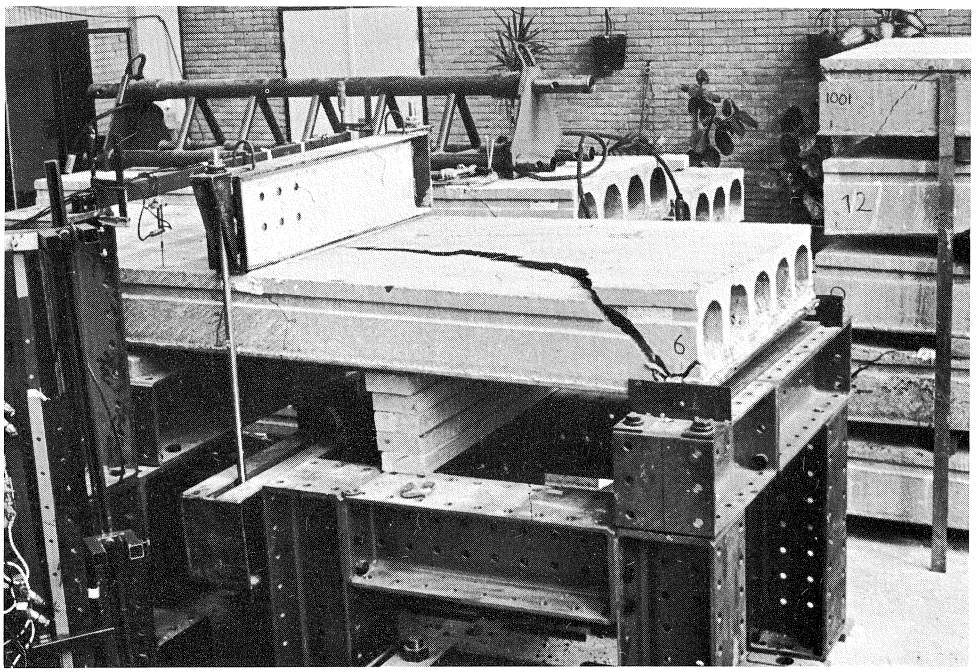

Fig. 4.12. Failure of specimen 6.

and 20): in specimen 8a only one strand, with the smallest initial slip, did not slip during the test. The specimen failed after rupture of this strand. In specimen 9 only one strand, with the largest initial slip, slipped during the test: the other strands ruptured. In 14 and 20 a few strands slipped, the others ruptured.

In all, 19 shear tension failures were observed, 18 of which were straight according to the definition given in Chapter 3.3. As mentioned earlier, specimen 6 displayed a complicated type of failure: at a load of $P = 250$ kN a longitudinal crack occurred at the bottom of the slab. This crack gave rise to a rather unusual type of failure (Fig. 4.12).

In the specimens 13 and 17 shear compression cracks occurred. The specimens failed, however, by rupture of all the strands, without any slip, so that these failures were classified as straight flexural failures.

5 Analysis of results

5.1 *Evaluation of theoretical lower bound expressions for series II*

In Chapter 3 the theoretical background of the possible failure modes has been dealt with. In this section the theoretical behaviour will be compared with the experimental findings, starting with series II.

Shear tension failure

Eq. (3.16) gives a practical formula for predicting the shear tension capacity. For a comparison with the experiments a prestress of $\sigma_p = 1150$ N/mm^2 is used (see Fig. 4.9), whereas a concrete splitting strength of $f_{ct} = 4.0$ N/mm^2 is used for the Dy-core and of 4.2 N/mm^2 for the Spiroll slabs. The dimensional properties of the specimens are given in Table 4.4. The support length was always $s = 100$ mm. For the $\frac{1}{2}''$ strands a transmission length of $l_t = 700$ mm is assumed, and for the $\frac{3}{8}''$ strands a value $l_t = 500$ mm. This results in values for α of 0.27 and 0.36, respectively.

The transmission lengths are slightly larger than might be expected on average (see, for example Fig. 4.11); this difference has a negligible influence on the theoretical shear tension capacity, whereas on the other hand uniformity with the anchorage failure criteria is obtained, where the same values for l_t and l_d are used.

A survey of all the specimens which failed in shear tension and their theoretical average shear tension capacity is given in Table 5.1.

It is found that for these 18 specimens an average value $V_{u,\mathrm{exp}}/V_{u,\mathrm{th}}$ of 0.91 is obtained, with a standard deviation of $s = 0.10$. Arguments to explain why the value $V_{u,\mathrm{exp}}/V_{u,\mathrm{th}}$ is smaller than 1 have already been given in Chapter 3.3.2. Table 5.1 shows that the SP 270 elements display higher values than the others. This could be due to the more favourable cross-sectional shape. A 5% lower bound for the shear tension capacity is found by using a reduction factor of 0.75 ($0.91 - 1.64 \times 0.10$). This is in good agreement with an analysis of results of tests by other authors, published in [20], where also 0.75 was found. Using this value in eq. (3.16) the full expression for the lower bound is:

Table 5.1. Experimental shear tension capacities, compared with values according to eq. (3.16)

type of slab	specimen	$V_{u,\mathrm{exp}}$ (kN)	$V_{u,\mathrm{th}}$ (kN)	$V_{u,\mathrm{exp}}/V_{u,\mathrm{th}}$
H 300-5	7a	216.0	254.3	0.85
	7b	231.5	254.3	0.91
	8b	181.6	254.3	0.71
H 300-10	10	208.5	280.8	0.74
	11a	224.6	280.8	0.80
	11b	239.3	280.8	0.85
	12	226.2	280.8	0.81
T 260-10	4a	284.3	288.4	0.99
	4b	268.3	288.4	0.93
	5a	286.3	288.4	0.99
	5b	252.1	288.4	0.87
T 260-6	15a	234.2	266.7	0.88
	15b	258.3	266.7	0.97
	16a	245.9	266.7	0.92
	16b	282.0	266.7	1.06
SP 270-13	18	240.6	260.4	0.93
	19a	276.3	260.4	1.07
	19b	263.9	260.4	1.02

$$V_{uk} = 0.75 \frac{Ib_w}{S} \sqrt{f_{ct}^2 + \alpha \cdot \sigma_N \cdot f_{ct}} \tag{5.1}$$

Shear compression failure

For the shear compression capacity a theoretical 5% lower bound value is readily available, so there is no need to consider mean values. The shear compression capacity was formulated in Section 3.4 as:

$$V_{uk} = 0.068 b_w \cdot d \cdot \xi \,(1 + 0.5\varrho_0)\sqrt{f_c} + \frac{M_0}{a} \tag{5.2}$$

where the decompression moment M_0 can be calculated from:

$$M_0 = A_p \cdot \sigma_p \left(e + \frac{W_0}{A_c}\right) \tag{5.3}$$

where e = the eccentricity of the strands.

Table 5.2. Theoretical characteristic shear compression capacities

type	V_{uk} (shear compression) (kN)
T 260-6	61.1 + 104.5/a
T 260-10	73.3 + 174.3/a
H 300-5	55.8 + 101.2/a
H 300-10	71.7 + 199.5/a
SP 270-13	60.4 + 126.9/a

f_c is the cylinder compressive strength of the concrete, which is taken here as equal to $f_c = 0.8 \times 60 = 48$ N/mm^2.

The 5% values for the shear compression capacity of the specimens tested in the experimental program are represented in Table 5.2.

Anchorage failure

A lower limit for the anchorage capacity can be established by using the critical steel stress envelope (eq. (3.3) and (3.4)).

According to Fig. 3.5 the flexural capacity should be reached if $a > l_d$. For $l_{cr} < a < l_d$ the anchorage capacity can be simply established by taking the internal lever arm as equal to the effective depth minus half the depth of the area beyond the cavities and reading the ultimate stress in the steel from the diagram in Fig. 3.4. For $a < l_{cr}$ failure occurs immediately upon flexural cracking. In this area a lower limit for the bearing capacity of the slabs in the tests is obtained by taking the 5% lower limit for the cracking moment. The cracking moment is equal to:

$$M_r = M_0 + W \cdot f_{ctf} \tag{5.4}$$

where M_0 is obtained from eq. (5.3).

An average value for the cracking moment is obtained by taking $f_{ctf} = 5.75$ N/mm^2 and substituting a steel stress of $\sigma_p = 1150$ N/mm^2 into the expression for M_0.

For the 5% lower limit of the cracking moment an estimated value of $0.90 M_{cr}$ is used.

By way of illustration the anchorage capacity for the elements H 300 with five $\frac{1}{2}''$ strands has been calculated as a function of the distance a between the load and the support.

H 300-5: $f_{ctf} = 5.75$ N/mm^2
$\sigma_p = 1150$ N/mm^2
$A_p = 5 \times 93 = 465$ mm^2
$A_c = 1.99 \times 10^5$ mm^2
$W_0 = 14.5 \times 10^6$ mm^2
$M_{fk} = 228$ kNm

The average cracking moment is (eq. (5.3) and (5.4)):

$$M_r = 465 \times 1150 \left(115 + \frac{14.5}{0.199}\right) + 14.5 \times 5.75 \times 10^6 = 183.8 \times 10^6 \text{ Nmm}$$
$$= 183.8 \text{ kNm}$$

so that $M_{rk} = 0.9 \times 183.8 = 165.4$ kNm.

The steel stress after flexural cracking is $\sigma_p + \Delta\sigma_p$. This is large enough to cause anchorage slip failure if:

$$z(\sigma_p + \Delta\sigma_p) \cdot A_p = M_{rk}$$

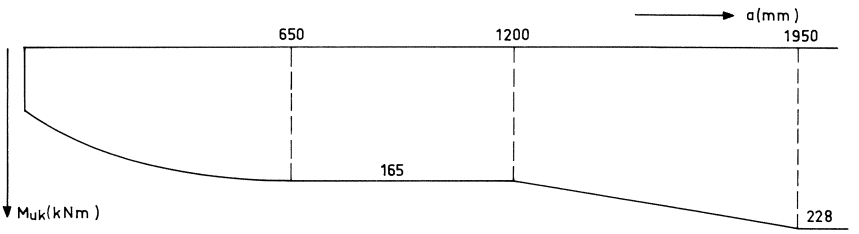

Fig. 5.1. Characteristic anchorage capacity for element H 300-5, as a function of the shear span a.

With $z = 260 - \frac{1}{2} \times 30 = 245$ it is found that $\sigma_p + \Delta\sigma_p = 1450$ N/mm^2, so that (Fig. 5.4) l_{cr} is found to be 1250 mm. This leads to the following conclusions:

for $a > l_d - \frac{1}{2}s$, or $a > 1950$ mm $M_{uk} = M_{fk}$
for $l_t - \frac{1}{2}s < a < l_{cr} - \frac{1}{2}s$, or $650 < a < 1200$ mm $M_{uk} = M_{rk} = 165.4$ kNm
for $a < l_t - \frac{1}{2}s$, or $a < 650$ mm $M_{uk} = M_{rkr}$, where M_{rkr} is the reduced cracking moment, due to the smaller prestress for $x < l_t$.

The characteristic bearing capacity with regard to anchorage failure is represented in Fig. 5.1.

Flexural failure

The principle for calculating the flexural capacity has been dealt with in Section 3.1. Adopting the values $f_c = 52$ N/mm^2, $\varepsilon'_p = 0.1\%$ and $\varepsilon'_u = 0.25\%$ (Fig. 3.1a) it is found that $\lambda = 0.81$ and $\beta = 0.41$. The characteristic tensile strength of the strands is $f_p = 1860$ N/m^2. The maximum support reaction is then:

$$V_{uk} = \frac{M_{uk}}{a} \tag{5.5}$$

The values calculated in this way are listed in Table 5.3.

Table 5.3. Flexural moment capacities

type	M_{uk} (kNm)
T 260-6	224.9
T 260-10	362.4
H 300-5	228.3
H 300-10	432.4
SP 270-13	273.2

In Table 5.4 the failure loads of all specimens are compared with the calculated theoretical lower bound values for the bearing capacities according to the criteria discussed earlier on. The following points should be noted:

If the load is applied at a distance smaller than l_d from the end face of the element, anchorage failure is decisive for the flexural behaviour: in that case the full flexural

Table 5.4. Experimental results and theoretical lower bound values (series II)

	experimental values				theoretical lower bound values				
test	type	a (mm)	$V_{u,\exp}$ (kN)	failure mode	shear tension (kN)	shear compression (kN)	anchorage failure (kN)	flexural failure (kN)	$\frac{V_{u,\exp}}{V_{uk,\text{th}}}$
1a	T 260-6	460	139.1	A	200.0	–	337	489	(0.70)*
1b	T 260-6	805	204.0	A	200.0	186	179	279	(1.14)*
2	T 260-6	1475	66.3	A	200.0	129	74.8	152	(0.89)*
3	T 260-6	1150	75.3	A	200.0	–	56.9	196	(1.32)*
13	T 260-6	1500	161.0	F	200.0	128	128.7	150	1.26
14	T 260-6	1150	186.0	A/F	200.0	148.5	143.5	196	1.30
15a	T 260-6	805	234.2	St	200.0	186	179	279	1.31
15b	T 260-6	460	258.3	St	200.0	264.5	298	489	1.29
16a	T 260-6	805	245.9	St	200.0	186	179	279	1.37
16b	T 260-6	460	282.0	St	200.0	264.5	298	490	1.41
4a	T 260-10	460	284.3	St	216.4	–	420	788	1.31
4b	T 260-10	805	268.3	St	216.4	280.3	290.8	450	1.24
5a	T 260-10	460	286.3	St	216.4	–	420	788	1.32
5b	T 260-10	1150	252.1	St	216.4	–	237	315	1.16
6	T 260-10	1500	213.3	St/L	216.4	184.2	208	242	1.16
7a	H 300-5	540	216.0	St	190.7	–	302	423	1.13
7b	H 300-5	945	231.5	St	190.7	–	175.1	242	1.32
8a	H 300-5	945	171.5	A	190.7	–	175.1	242	0.98
8b	H 300-5	440	181.6	St	190.7	–	357	519	0.95
9	H 300-5	1500	156.6	A/F	190.7	123.5	122.5	152	1.28
10a	H 300-10	540	208.5	St	210.6	–	465	801	0.99
10b	H 300-10	945	151.1	A	210.6	284	315	457	(0.72)*
11a	H 300-10	945	224.6	St	210.6	284	315	457	1.07
11b	H 330-10	540	239.3	St	210.6	–	465	801	1.14
12	H 300-10	1495	226.2	St	210.6	205.3	248.3	289	1.10
17	SP 270-13	1500	190.9	F	194.1	145.6	182	182	1.31
18	SP 270-13	1150	240.6	St	194.1	170.7	215	238	1.41
19a	SP 270-13	805	276.3	St	194.1	217	247	339	1.42
19b	SP 270-13	460	263.9	St	194.1	–	372	593	1.43
20	SP 270-13	1150	240.8	A/F	194.1	170.7	215	238	1.41

* downgraded elements, see Section 5.3

capacity is not of practical importance, but is nevertheless mentioned as additional information. The shear compression formula is in principle valid only for the region cracked in bending. So if the shear compression capacity is found to be smaller than M_{rk}/a, the region is uncracked, so that the value is unrealistic: in that case it is not mentioned.

Fig. 5.2 shows the ratio $V_{u,\exp}/V_{uk,\text{th}}$ for all tests, except the tests on the specimens which might have been expected to be downgraded on the basis of quality control criteria.

It is seen that the combination of criteria, as previously discussed, gives a good lower bound for the bearing capacity. Besides, the ratio $V_{u,\exp}/V_{uk,\text{th}}$ never exceeds the value 1.43, which shows that the margin of scatter is reasonably small.

Comparing the $V_{u,\exp}/V_{uk,\text{th}}$ values for the various types of specimens it is seen that the specimens of type SP 265 obviously have a higher safety than the T 260 slabs, which in their turn display a higher safety that the H 300 slabs. This is probably due to the geometrical differences between the various cross-sections (Fig. 4.6.). The SP slabs have circular holes so that a shear tension crack will preferably occur at mid-depth, within a limited area.

The T 260 slabs have ribs of more rectangular shape which enables the crack to occur at the weakest place within a larger area, which results in a lower shear tension capacity. The H 300 slabs display a sudden change in rib thickness just under the centroidal axis. From fracture mechanics it is known that in a material like concrete with limited deformation capacity the stress concentration occurring in a necked area results in a reduced true tensile strength.

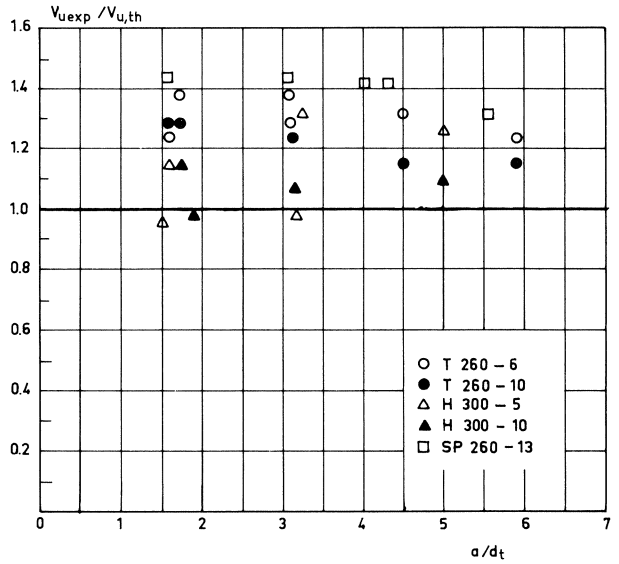

Fig. 5.2. Comparison between test results and theoretical lower bound capacities for the specimens of series II.

5.2 *The relation between the initial slip of the strands upon sawing and the transmission length*

Many precasting plants have a policy of downgrading (rejecting) slabs with large initial slip of the strands and approving slabs with small slip values. Therefore special attention is given to this matter.

The initial slip of the strands is the cumulative relative displacement which occurs between the steel and the concrete over the transmission area when the strands are sawn. Hence the value of this slip is theoretically equal to the differential strain. If transfer takes place linearly, the relative displacement should be equal to the product of the transfer length l_t and the average differential strain (Fig. 5.3a).

$$\delta = \tfrac{1}{2} l_t \cdot \frac{\sigma_{pi}}{E_s} \tag{5.6}$$

For $\frac{1}{2}''$ strands, with $l_t = 700$ mm and $\sigma_{pi} = 1265$ N/mm^2 (as measured in the factory), δ should be 2.2 N/mm^2. This is significantly larger than was measured (Table 4.8) on the test specimens. Even if it were assumed that the stress in the strands develops according to a second-order parabola (Fig. 5.3b), and a value of $l_t = 500$ mm were adopted, the value of δ would be as much as 1.1 mm, which is still 2.5 times the average actually measured value.

It is probable that the sawing process is responsible for this difference. Quite conceivably the response of the concrete (unstressed, heterogeneous, brittle, relatively low modulus of elasticity) is different from that of the strands (stressed, homogeneous, ductile, relatively high modulus of elasticity). This could mean that the initial slip of the strands is not merely the cumulative relative displacement between steel and concrete but is actually smaller due to the comparatively thick layer of concrete lost during sawing.

The assumption that the sawing process affects the magnitude of the initial slip is supported by the observations described in 4.2.5 (Fig. 4.10 and 4.11). Whereas the transmission length was found to be about 500 mm on both sides of the saw cut the average initial slip values of six strands were respectively $\delta_{av} = 0.79$ mm, with a standard deviation of $s = 0.16$ mm, for specimen 15 and $\delta_{av} = 0.18$ mm, with $s = 0.14$ mm, for specimen 16.

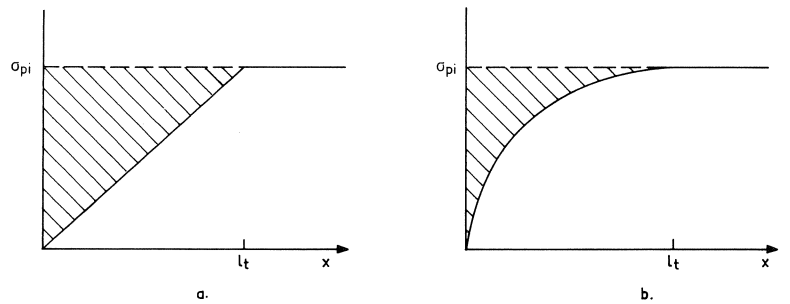

Fig. 5.3. Calculation of initial slip of the strands, linear (a) and parabolic (b).

It can be concluded that formulas relating the transmission length to the initial slip obviously do not apply to specimens with end faces formed by sawing.

5.3 *The behaviour of the downgraded elements*

Of special interest is the behaviour of the elements 1-3, which all failed by pull-out of the strands at relatively low loads.

In Section 3.2 envelopes of the limiting the stress in the steel at the ends of the units to prevent pull-out failure have been indicated (Fig. 3.3). Eq. (3.3) and (3.4) were used for the evaluation of the results. According to Anderson [3] this envelope is valid for strands which have an initial slip not larger than

$$\delta_{\text{lim}} = \frac{\sigma_{pi}\phi}{6650} \text{ (N, mm)} \tag{5.7}$$

For $\frac{1}{2}''$ strands, with an average initial prestress of $\sigma_{pi} = 1265$ N/mm^2, it is found that $\delta_{\text{lim}} = 2.4$ mm. For larger values of the initial slip reduction factors for the allowable steel stress are proposed in [3]. These factors depend on the amount of slip, the nominal diameter of the strand and the development length. The values are given in Table 5.5.

Table 5.5. Capacity reduction factors for prestressing strands [3]

	$\delta/\delta_{\text{lim}}$			
$l_d/100\phi$	1.0-1.5	1.5-2.0	2.0-2.5	2.5 +
1-2	0.60	0.40	0.20	0
2-2.5	0.80	0.60	0.40	0.20
2.5-3	1.00	0.80	0.60	0.40

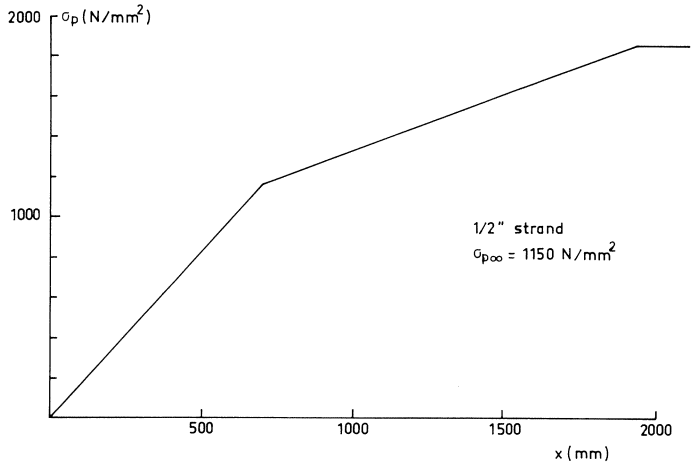

Fig. 5.4 Pull-out stress envelope according to eq. (3.3) and (3.4).

For specimens 2 and 3, with initial slip values of 2.9 and 3.8 mm, and $l_d = 1970$ mm (according to eq. (3.4)) reduction values of respectively 0.60 and 0.40 are obtained. In specimen 2 the allowable stress under the load, at a distance of

$$1475 + \frac{100}{2} = 1525 \text{ mm}$$

from the sawn end, is $\sigma_{pu} = 1610$ N/mm^2 (see Fig. 5.4). Using the reduction factor 0.6, it is found that σ_{pu} becomes 965 N/mm^2. So the lower bound moment for pull-out of the strands is:

$$M = A_p \cdot \sigma_{pu}(d - 20) = 6(93)965(225 - 20) = 110.4 \text{ kNm},$$

which is associated with a support reaction

$$V = \frac{110.4}{1.475} = 74.8 \text{ kN}$$

In the test it was observed that pull-out of the strands occurred at $V_s = 62.3$ kN, after the formation of a flexural crack at $V = 66.3$ kN (Table 4.8).

A survey of the values for all the tests 1-3 is given in Table 5.6.

Table 5.6. Comparison between experimental values and pull-out criteria

	experimental values				theoretical values			
test	a (mm)	δ_{av} (mm)	V_u (kN)	V_s (kN)	reduction factor	σ_p (N/mm^2)	V_s (kN)	$\frac{V_{s,\text{exp}}}{V_{s,\text{th}}}$
1a	460	0.1	139.3	118	1	840	209	0.56
1b	805	0.0	204	204	1	1235	175.5	1.16
2	1475	2.9	66.3	62.3	0.6	965	74.8	0.83
3	1150	3.8	75.3	75.3	0.4	572	56.9	1.32

It can be concluded that the use of a capacity reduction factor as given in Table 5.6 is not sufficient to ensure a safe calculation of the pull-out capacity. This is specially evident on comparing the results of the tests 1a and 1b, carried out on both sides of the same element, which apparently had a high concrete quality (Table 4.5 and 4.6). Nevertheless the results of the tests reveal a significant difference in anchorage capacity.

This shows that control of the initial slip of the strands may be considered as not more than one aspect of quality control, which should further include accurate control of the compaction (shrinkage cracking, etc.). Especially if somewhere on a casting bed large initial slip of strands is observed, the other parts should be checked with utmost care. It is moreover advisable regularly to carry out tests on the slabs in order to monitor the manufacturing process.

5.4 *Comparison of theoretical lower bound values for series I*

For the sake of completeness the theoretical lower bound values have also been com-

pared with the experimental results of the tests on specimens 1-9 of series I which predominantly failed in flexure (Table 4.3).

A comparison between the experimental and the theoretical lower bound values is given in Table 5.7. The properties of the slabs are found in Section 4.1.

Table 5.7. Experimental results and theoretical lower bound values (series I)

specimen	a (mm)	$V_{u,\exp}$ (kN)	failure mode	shear tension	shear compression	anchorage failure	flexural failure	$\frac{V_{u,\exp}}{V_{uk,th}}$
1	1800	61.7	F	202	87.8	-	57.7	1.07
2	2500	44.0	F	202	80.1	-	41.6	1.06
3	3000	36.0	F	202	76.8	-	34.7	1.04
4	1500	78.1	F	202	93.4	-	69.4	1.13
5	1000	113.2	F	202	109.8	87.5	104.1	1.09
6	750	150.9	F	202	126.2	116.7	138.8	1.29
7	500	221.0	F/A	202	-	175	208.1	1.26
8	500	314	F/A	216	-	200.2	326.4	1.57
9	375	276.5	F	202	-	233	277.5	1.37

Only in the case of specimen 8, which has 11 strands instead of 7, does the ratio $V_{u,\exp}/V_{uk,th}$ seem to be conservative.

5.5 *Consequences for the design*

The expressions (5.1) and (5.2) are directly suited as a basis for design equations.

With regard to the anchorage capacity a number of regions were distinguished. For cross-sections at distances $> l_d$ the full flexural capacity is reached. For the region $l_{cr} < x < l_d$ slip of the strands will occur at a bending moment which is larger than the flexural cracking moment. However, for $x < l_{cr}$ anchorage failure will occur directly after flexural cracking. For normal loading configurations such as uniformly distributed loading it will, to ensure safety, be sufficient to require that at a distance l_{cr} from the end of the slab the flexural cracking moment will not be reached when the design moment is applied. In the particular case where concentrated loads are applied at $x < l_{cr}$ the concrete should be regarded as cracked in bending, and the moment at which the strands actually slip should be regarded as the governing criterion.

6 Summary and conclusions

As regards the behaviour of prestressed hollow core slabs, four different failure modes can be distinguished, two of the flexural and two of the shear type. With regard to the behaviour in flexure a distinction can be made between pure flexural failure, where the bearing capacity is limited by the strength of the prestressing steel, and anchorage failure, where the strands are pulled out of the concrete before rupture of the strands can occur. As far as the behaviour in shear is concerned two failure modes can occur. A shear crack can develop from a flexural crack and reduce the compression area to such an extent that it fails: this type of failure is called shear compression failure. Further-

more, shear failure can occur in the region uncracked in flexure if the concrete tensile strength, at about mid-depth of the ribs, is reached. This failure type is called shear tension failure.

In order to find safe lower bound expressions for the bearing capacity, two series of tests were carried out. Variables were the geometry and depth of the cross-section ($200 < d_t < 300$ mm), the shear span to depth ratio ($1.7 < (a/d_t) < 18.7$), the diameter of the prestressing strands ($\phi = 9.3$ and 12.6 mm) and the total prestressing force (average concrete compressive stress in the cross-section $2.7 < \sigma_N < 4.4$ N/mm^2). Altogether there were 19 shear tension failures, seven anchorage failures and 10 pure flexural failures; in five tests combined flexural/anchorage failures occurred. No shear compression failures occurred in spite of the incidental formation of pronounced shear-flexure cracks (Fig. 2.5). A 5% lower limit for the shear tension capacity was calculated from:

$$V_{uk} = 0.75 \frac{I \cdot b_w}{S} \sqrt{f_{ct}^2 + \alpha \cdot \sigma_N \cdot f_{ct}}$$

where f_{ct} is the average concrete splitting strength, σ_N is the average concrete compressive stress in the region where the prestressing force is fully introduced into the concrete ($\sigma_N = \sigma_p \cdot (A_p/A_c)$) and α is the fraction of the prestress at the inner edge of the support in relation to the full prestress in the strands.

As a lower limit for shear compression failure the expression

$$V_{uk,x} = 0.068 b_w \cdot d \left(1 + 0.5 \frac{100 A_s}{b_w \cdot d}\right) \sqrt{f_c} + \frac{M_0}{M_x/V_x}$$

can be used. This is the basic equation from which the shear formula in the actual CEB Model Code was derived. In the authors' opinion the basic equation is more suitable than the official one. In tests by other authors [10] shear compression failures are reported, so that this equation should in any case be taken into account. The equation is principally valid for the area cracked in flexure.

With regard to pure flexural and anchorage "pull-out" behaviour it is sufficient to limit the stress in the prestressing steel. The current approach as described in the ACI Recommendations [1] appeared to give adequate results; here the transmission length l_t is formulated as:

$$l_t = \frac{\sigma_{p\infty} \cdot \phi}{21}$$

whereas the development length is equal to:

$$l_d = l_t + \frac{(f_p - \sigma_{p\infty})}{7} \cdot \phi$$

For cross-sections at distances $> l_d$ from the sawn end-face the full characteristic tensile strength of the steel f_p is reached. For $l_t < x < l_d$ the limit value is calculated by interpolating between the effective prestress in the strands $\sigma_{p\infty}$ and f_p. For $0 < x < l_t$ an inter-

polation between 0 and $\sigma_{p\infty}$ should be carried out. This procedure is valid if the initial slip of the strands, upon sawing, is not larger than an empirical value

$$\delta_{\text{lim}} = \frac{\sigma_{pi} \cdot \phi}{6650},$$

which is roughly 0.2 times the strand diameter. Capacity reduction factors for slip values larger than δ_{lim}, as proposed in [3], did not give safe results.

Measurements of the concrete strain before and after sawing showed that there is no distinct relation between the initial slip and the transmission length, which is obviously due to the process of sawing. Besides, it was found that a high concrete strength does not necessarily guarantee good anchorage capacity. This capacity depends mainly on the compaction of the concrete around the strands.

These observations emphasise the need for well-defined quality control criteria and procedures.

Comparing the theoretical lower bound values with the experimental results it was found that, for nearly all the tests, values between 1.0 and 1.4 were found for $V_{u,\text{exp}}/V_{uk,\text{th}}$.

Two slabs were subjected to concentrated loads at midspan, one applied centrically and one eccentrically. The object of these tests was to investigate to what extent a concentrated load produces a non-uniform distribution of the strains or deflections and thus brings about a more specific type of failure. The results indicate that the slab possesses sufficient torsional stiffness, so that it cracks and fails almost as though it were subject to a linear or a uniformly distributed load. One test was carried out on a double slab, coupled by a transverse joint. One of the slabs was loaded, whereas the adjacent slab remained unloaded. At their ends the slabs were interconnected by small beams cast in situ. It was concluded that very good load spread is achieved as a result of the considerable torsional stiffness of the slabs. Since the flexural stiffness of the slabs greatly decreases after the cracking moment has been attained, the non-loaded slab will from then onward carry an even larger share of the load.

7 Acknowledgements

The authors wish to thank the slab producers for kindly supplying the test specimens free of charge. Especially the helpful cooperation given by Mr. Vermeiden and Mr. De Wit of Dy-Core Systems and by Mr. Peters of Schokbeton is gratefully acknowledged.

8 Notation

a	shear span
b	total width of element
b_w	total width of all ribs at smallest section
d	effective depth
d_t	full depth
e	eccentricity of prestressing strands

f_c	concrete cylinder compressive strength
f_{cc}	concrete cube compressive strength
$\bar{f}_{cc}$	average concrete cube compressive strength
f_{ci}	concrete strength at (initial) transfer
f_{ct}	concrete splitting tensile strength
f_{ctf}	concrete flexural tensile strength
f_p	rupture strength of prestressing steel
f_{pk}	characteristic rupture strength of prestressing steel
l	length
l_{cr}	distance from end face to cross-section where flexural cracking load is equal to anchorage (pull-out) capacity
l_d	development length
l_t	transmission length
s	width of bearing plate
x	depth of compression zone
z	internal lever arm
A_c	cross-sectional area of steel
A_p	cross-sectional area of prestressing steel
I	moment of inertia
M	flexural moment
M_0	decompression moment
M_r	flexural cracking moment
M_{rk}	characteristic cracking moment
M_u	ultimate moment
M_{uk}	characteristic flexural moment
M_x	flexural moment at distance x from bearing
P	load
P_u	ultimate load
S	static moment
V	shear force
V_s	maximum shear force developed at slip of strands
V_u	ultimate shear force
$V_{u,\mathrm{exp}}$	ultimate shear force in experiment
$V_{u,\mathrm{th}}$	ultimate shear force according to theory
V_x	shear force at distance x from bearing
W	section modulus
α	fraction of prestress in cross-section considered
β	distance factor for concrete compression zone
δ	initial slip of strands upon sawing
δ_{av}	average value of δ
δ_{lim}	limit value of δ for which eq. (3.3) and (3.4) apply
ϕ	diameter of strand
ϱ	reinforcement ratio

ϱ_0	reinforcement percentage
λ	shape factor for concrete compression diagram
σ_{cxx}	stress in concrete parallel to x-axis
σ_{cyy}	stress in concrete parallel to y-axis
σ_{cxy}	shear stress in concrete parallel to x- or y-axis
σ_N	average concrete compressive stress in cross-section
σ_p	prestress in strands
σ_{pi}	initial prestress in strands
$\sigma_{p\infty}$	prestress in strands after all losses

9 References

1. ACI Committee 318, Building Code Requirements for Reinforced Concrete, (ACI 318-71), American Concrete Institute, Detroit, 1971.
2. AL-KUBAISY, M. A. and A. G. YOUNG, Failure of concrete under sustained tension, Magazine of Concrete Research, Vol. 27, No. 92, pp. 171–181, September 1975.
3. ANDERSON, A. R. and R. G. ANDERSON, An Assurance Criterion for Flexural Bond in Pretensioned Hollow Core Units, ACI-Journal, Proceedings, Vol. 73, No. 8, August 1976, pp. 457–464.
4. BOOGAARD, W. J. VAN DEN, Demonteerbaar bouwen, Cement 33 (1981), No. 6, pp. 363–367.
5. CUR, Splitting strength of high-strength concrete, Report No. 52, The Netherlands, 1971 (in Dutch).
6. FOURÉ, B., Résistance du béton sous contrainte soutenu, Matériaux et Constructions, RILEM, Vol. 00, pp. 110–121, June 1982.
7. GERSTNER, R. W. and J. H. WRONKIEWICZ, Pretension anchorage stresses, Proc. ASCE, Struct. Div., Vol. 95, No. ST 9, 1969.
8. HEDMAN, O. and A. LOSBERG, Design of concrete structures with regard to shear forces, CEB Bulletin No. 126, June 1978, pp. 184–209.
9. HUYGHE, G. F., J. C. WALRAVEN and J. STROBAND, Research on extruded concrete hollow core slabs, Stevin Report 5-80-2, Delft University of Technology, November 1980.
10. KAMERLING, J. W. and H. J. FIJNEMAN, Onderzoek holle prefab vloerplaten, Eindhoven University of Technology, The Netherlands, August 1980.
11. KUPFER, H., H. K. HILSDORF and H. RÜSCH, Behaviour of concrete under biaxial stresses, ACI-Journal, Vol. 66, August 1969, pp. 656–666.
12. MARTIN, L. D. and N. L. SCOTT, Development of Prestressing Strand in Pretensioned Members, ACI-Journal, Proceedings, Vol. 73, No. 8, August 1976, pp. 453–456.
13. MERCX, W. P. M., The shear capacity of prestressed hollow core slabs, Master's Thesis, Delft University of Technology, The Netherlands, 1982.
14. MITCHELL, N. B., The indirect tension test for concrete materials, Materials Research and Standards, October 1961.
15. PETERS, M. H. W., Praktijk en mogelijkheden van demonteerbaar bouwen, Cement 33 (1981), No. 6, pp. 375–376.
16. PLÄHN, J. and K. KRÖLL, Spannungsverteilung im Eintragungsbereich des Spannbetonbalkens mit unmittelbarem Verbund, Beton- und Stahlbetonbau, Vol. 70, No. 7, 1975, pp. 170–175 and No. 8, 1975, pp. 188–194.
17. REINHARDT, H. W., Demontabele Betongebäude, Cement 28 (1976), No. 6, pp. 266–273.
18. REINHARDT, H. W., Demountable Precast Concrete Structures, Proceedings of the Ninth International Congress of the FIP, Stockholm, June 1982, Vol. 1, pp. 86–94.
19. WARD, P., Shear tests on Spiroll units, Report on tests carried out at Richard Lees Company, England, October 1980.

20. WALRAVEN, J. C., The shear resistance of prestressed hollow core slabs, FIP Technical Paper "Design principles for hollow core slabs regarding shear and transverse load-bearing capacity, splitting and quality control", October 1982.
21. ZIA, P. and T. MOSTAFA, Development Length of Prestressing Strand, PCI-Journal, Vol. 22, No. 5, September-October 1977, pp. 54–65, and Discussion, PCI-Journal, No. 4, July-August 1978, pp. 97–107.